Sensitivity analysis of thickness assumptions for piezoelectric plate models

M. d'Ottavio, O. Polit

Sensitivity Analysis of Thickness Assumptions for Piezoelectric Plate Models

MICHELE D'OTTAVIO* AND OLIVIER POLIT

Laboratoire Energétique, Mécanique et Electromagnétisme (LEME)
Université Paris Ouest, 50 rue de Sèvres, 92410 Ville d'Avray, France

INTRODUCTION

PIEZOELECTRIC sensors and actuators are increasingly used in intelligent structures because their characteristics meet many requirements posed by relevant technical applications, for instance active vibration damping, health monitoring, or shape adaptation (Chopra, 1996, 2002). Piezoelectric patches can be conveniently attached to or embedded into a hosting structure depending on the exploited actuation mode. The design of intelligent structures demands accurate numerical studies because an experimental try-and-error procedure is often excessively time-comsuming and expensive. Due to the complexity of practically relevant components, approximate structural models for beams, plates and shells are usually employed in the numerical simulations.

There are several ways to formulate approximate structural models. One possibility is to rationally derive them upon taking the thin plate limit of the full 3D equations governing the piezoelectric continuum (Maugin and Attou, 1990; Rogacheva, 1994; Bisegna and Maceri, 1996a,b). Thanks to the direct deduction from full 3D equations, this approach ensures consistency and permits to estimate the approximation error (Cheng et al., 2000; Reddy and Cheng, 2001). However, this method has been usually restricted to formulate low-order plate or shell models, whose applicability is limited to quite thin patches and low-frequency response.

An alternative way to construct structural models refers to the more intuitive 'axiomatic' approach, by which the through-thickness behavior of the field variables is *a priori* postulated on the basis of 'reasonable' assumptions (Naghdi, 1972). The axiomatic approach has encountered a broad success thanks to its mathematical manageability that permits a straightforward formal application to complex problems, in particular multilayered structures and multiphysical coupling. Despite its attractive simplicity, this modeling technique is subject to a certain arbitrariness reflected in the choice of hypotheses concerning the behavior of mechanical and electrical field variables (Gopinathan et al., 2000). A vast amount of literature has been accordingly dedicated to axiomatic models with differently chosen thickness assumptions, and the following overview has by no means the aim of being exhaustive.

Wang and Yang (2000) summarized a large number of axiomatic models for piezoelectric plates and classified them with respect to their applicability for the analysis of transducers working in different frequency ranges. Reddy (1999) and Robbins and Chopra (2006) proposed various models for the simulation of multilayered panels with piezoelectric actuators. They discussed classical and

*Author to whom correspondence should be addressed.
E-mail: michele.d_ottavio@u-paris10.fr
Figures 2 and 12 appear in color online: http://jim.sagepub.com

refined single layer as well as layer-wise kinematic assumptions by referring to the hypothesis of a constant electric field. Based on the same assumption for the electrical field, Mannini and Gaudenzi (2004) extended the hierarchic approach of Gaudenzi et al. (1995, 1998) to formulate finite elements for piezo-actuated laminates. Since in these models the converse piezoelectric effect is assumed to be negligible, the electrical field variables do not explicitly appear as additional unknowns. However, the review articles of Saravanos and Heyliger (1999) and Benjeddou (2000) pointed out the importance of retaining an adequate approximation for the electric degrees of freedom to consistently represent the piezoelectric interaction, in particular for sensor applications. Hence, Sze et al. (2004) and Polit and Bruant (2006) compared different approximations for the electric degrees of freedom within a multilayered model based on Reissner–Mindlin kinematics. Similarly, Pietrzakowski (2008) compared the vibration response of piezoelectric Kirchhoff and Reissner–Mindlin laminates with linear and quadratic assumptions for the electrostatic potential. A refined kinematic model involving higher-order trigonometric expansions for the electrostatic potential has been formulated by Fernandes and Pouget (2001) for homogeneous piezoelectric plates and subsequently extended to laminates upon accounting for electro-mechanical interfaces (Fernandes and Pouget, 2002).

While the literature mentioned above is focussed on the so-called extension mode (31 mode) of transversely polarized patches, shear-actuated piezoelectric elements are attracting interest since the pioneering works of Sun and Zhang (1995), Zhang and Sun (1996, 1999), Benjeddou et al. (1997), and Trindade et al. (1999). This actuation mode is based on the transverse shear deformation, which makes the classical Kirchhoff assumption of a vanishing shear stress meaningless (Vel and Batra, 2001a). Since shear-actuated elements are usually embedded into a smart sandwich structure (Baillargeon and Vel, 2005), models based on first-order shear deformation theory (Raja et al., 2004) have been enhanced by formulating higher-order kinematics to resolve transverse shear effects and cross-section warping (Aldraihem and Khdeir, 2003). Trindade and Benjeddou (2006, 2008) recently proposed a third-order sandwich beam theory that retains a cubic approximation for the electrostatic potential.

Classical plate theories are usually based on the hypothesis of a transverse deflection that remains constant through the thickness. This calls for the use of the reduced constitutive law for enforcing the condition of a vanishing transverse normal stress (Bhaskar and Varadan, 2001). Reduced constitutive coefficients have been employed in several of the already mentioned higher-order models (Reddy, 1999; Fernandes and Pouget, 2001, 2002; Raja et al., 2004; Trindade and Benjeddou, 2006, 2008). However, the available exact solutions for piezoelectric laminates working in extension (Heyliger and Brooks, 1996; Heyliger, 1997) and in shear mode (Benjeddou and Deü, 2001; Vel and Batra, 2001b) show that the transverse normal deformation plays a more relevant role compared to purely elastic laminates. Hence, refined axiomatic models for problems involving coupled multiphysics (in particular piezoelectricity and thermo-mechanics) have been proposed based on the full 3D constitutive relation by e.g. Batra and Vidoli (2002), Cho and Oh (2003), and Kant and Shiyekar (2008). If full 3D constitutive laws are retained, the kinematic model should be carefully chosen in order to avoid a spurious stiffening mechanism known as Poisson locking (Büchter et al., 1994; Carrera and Brischetto, 2008a,b).

In the last years, a family of axiomatic models has been developed for laminated plates and shells with piezoelectric layers (Ballhause et al., 2005; D'Ottavio and Kröplin, 2006; D'Ottavio et al., 2006, 2008; Carrera and Brischetto, 2007a,b). Thanks to a compact notation known as Carrera's Unified Formulation (CUF), a large number of models can be constructed within one single software (Carrera, 2000, 2003). Since these theories retain the full 3D constitutive law, the most refined models of CUF can accurately recover the exact 3D solutions, as demonstrated in the quoted references. In CUF, the field variables are grouped together as displacements, transverse stresses, electrostatic potential, and transverse electric displacement, and all variables are expanded in the thickness direction with polynomials of the same order N. A similar approach to the analysis of elastic plates has been proposed by Batra et al. (2002), in which a series of K-th order theories has been constructed based on the mixed Hellinger–Reissner functional by introducing assumptions of order K for the displacements and in-plane stresses and $(K+2)$ for the transverse stresses (with $K \in (1, 5)$). Recently, Demasi (2008) extended the flexibility of CUF for elastic laminates by permitting different polynomial orders for each single displacement component. This so-called Generalized Unified Formulation (GUF) is thus a powerful means to thoroughly assess the role of each single thickness assumption on the overall accuracy of the plate model. Moreover, the GUF can be conveniently employed to find the axiomatic model that maximizes the ratio between accuracy and required computational effort for a specific problem.

In this work, the basic ideas of the GUF are extended to the analysis of homogeneous piezoelectric plates. Within the classical variational formulation of Tiersten (1969), independent polynomial assumptions are introduced for in-plane displacements, transverse displacement, and electrostatic potential. Either the full 3D constitutive law or the reduced constitutive

coefficients can be utilized for the extension and the shear actuation modes. Therefore, a large number of axiomatic plate theories for piezoelectric actuator and sensor applications are constructed. These models are then assessed with respect to their capability to represent the coupled piezoelectric response of various actuator and sensor configurations. The GUF appears hence as a natural tool for assessing 2D models because it permits to systematically compare all terms of the approximated coupled piezoelectric behavior.

An outline of the article is as follows. The governing equations for the piezoelectric continuum are recalled in section 'Equation of a 3D Piezoelectric Continuum'. Section 'The Piezoelectric GUF' introduces the axiomatic plate models obtained by the piezoelectric GUF and their Navier-type analytical solution. The effects of an inconsistent kinematic model in conjunction with a full 3D constitutive law are exemplarily shown in Section 'Linear Elastic Plates' for linear elastic plates by addressing the well-known Poisson locking. Sections 'Piezoelectric Plate Working In 31-Mode' and 'Piezoelectric Plate Working In 15-Mode' present results for piezoelectric actuators and sensors working in extension and shear mode, respectively. Section 'Conclusions and Outlook' summarizes the principal findings, identifies model recommendations and suggests an outlook towards further investigations.

EQUATIONS OF A 3D PIEZOELECTRIC CONTINUUM

The governing equations for a piezoelectric continuum describe the mechanical field and electrical field as well as the constitutive law representing the piezoelectric interactions. For both fields, equilibrium of the intensive variables (i.e., the mechanical stresses σ_{ij} and the electric displacement D_i) is expressed by divergence equations, while the extensive variables (i.e., the mechanical strains ϵ_{ij} and the electric field E_i) are defined by gradient equations. The set of partial differential equations is closed by conditions defined on the domain boundary $\Gamma = \Gamma_u \cup \Gamma_t = \Gamma_\Phi \cup \Gamma_q$ by prescribing values for the displacement u_i and the electrostatic potential Φ or for the traction t_i and the electric charge density q (Tiersten, 1969):

- Mechanical field:

$$\frac{\partial \sigma_{ij}}{\partial x_i} = \rho \ddot{u}_j; \quad \epsilon_{ij} = \frac{1}{2}\left(\frac{\partial u_i}{\partial x_j} + \frac{\partial u_j}{\partial x_i}\right); \tag{1a}$$

$$u_i = \bar{u}_i \quad \text{on } \Gamma_u; \quad \sigma_{ij} n_j = \bar{t}_i \quad \text{on } \Gamma_t. \tag{1b}$$

- Electrical field:

$$\frac{\partial D_i}{\partial x_i} = 0; \quad E_i = -\frac{\partial \Phi}{\partial x_i}; \tag{2a}$$

$$\Phi = \bar{\Phi} \text{ on } \Gamma_\Phi; \quad D_i n_i = -\bar{q} \text{ on } \Gamma_q. \tag{2b}$$

The standard Einstein tensor notation has been used with the indexes i, j being defined in the set $\{1, 2, 3\}$. The domain is described by the Cartesian coordinates $x_i = \{x, y, z\}$, z being the thickness direction of the plate. The mass density has been indicated by ρ, the symbol n_i stays for the cosine director of the outward normal to the domain boundary, and prescribed values have been indicated by a bar.

The piezoelectric interactions depend on the polarization scheme and on the actuation mode. In this work, we refer to the transverse extension mode associated to a thickness polarization and to the transverse shear mode associated to an in-plane (first axis) polarization. In either case, the typical patch configuration is considered, with electrode-covered top and bottom faces of the plate and an electric field that is built up along the plate thickness. The full 3D constitutive equations describing the direct (sensor) and converse (actuator) piezoelectric effect read:

- Extension mode (31-mode, polarization along $x_3 = z$):

$$D_x = \varepsilon_{11} E_x + e_{15} \epsilon_{xz}; \quad D_y = \varepsilon_{22} E_y + e_{24} \epsilon_{yz}; \tag{3a}$$

$$D_z = \varepsilon_{33} E_z + e_{31} \epsilon_{xx} + e_{32} \epsilon_{yy} + e_{33} \epsilon_{zz}. \tag{3b}$$

$$\sigma_{xx} = \tilde{C}_{11} \epsilon_{xx} + \tilde{C}_{12} \epsilon_{yy} + \tilde{C}_{13} \epsilon_{zz} + \tilde{C}_{16} \epsilon_{xy} - e_{31} E_z; \tag{4a}$$

$$\sigma_{yy} = \tilde{C}_{21} \epsilon_{xx} + \tilde{C}_{22} \epsilon_{yy} + \tilde{C}_{23} \epsilon_{zz} + \tilde{C}_{26} \epsilon_{xy} - e_{32} E_z; \tag{4b}$$

$$\sigma_{zz} = \tilde{C}_{31} \epsilon_{xx} + \tilde{C}_{32} \epsilon_{yy} + \tilde{C}_{33} \epsilon_{zz} - e_{33} E_z; \tag{4c}$$

$$\sigma_{yz} = \tilde{C}_{44} \epsilon_{yz} - e_{24} E_y; \quad \sigma_{xz} = \tilde{C}_{55} \epsilon_{xz} - e_{15} E_x; \tag{4d}$$

$$\sigma_{xy} = \tilde{C}_{61} \epsilon_{xx} + \tilde{C}_{62} \epsilon_{yy} + \tilde{C}_{66} \epsilon_{xy}. \tag{4e}$$

- Shear mode (15-mode, polarization along $x_1 = x$):

$$D_x = \varepsilon_{11} E_x + e_{11} \epsilon_{xx} + e_{12} \epsilon_{yy} + e_{13} \epsilon_{zz}; \tag{5a}$$

$$D_y = \varepsilon_{22} E_y + e_{26} \epsilon_{xy}; \quad D_z = \varepsilon_{33} E_z + e_{35} \epsilon_{xz}. \tag{5b}$$

$$\sigma_{xx} = \tilde{C}_{11} \epsilon_{xx} + \tilde{C}_{12} \epsilon_{yy} + \tilde{C}_{13} \epsilon_{zz} + \tilde{C}_{16} \epsilon_{xy} - e_{11} E_x; \tag{6a}$$

$$\sigma_{yy} = \tilde{C}_{21} \epsilon_{xx} + \tilde{C}_{22} \epsilon_{yy} + \tilde{C}_{23} \epsilon_{zz} + \tilde{C}_{26} \epsilon_{xy} - e_{12} E_x; \tag{6b}$$

$$\sigma_{zz} = \tilde{C}_{31} \epsilon_{xx} + \tilde{C}_{32} \epsilon_{yy} + \tilde{C}_{33} \epsilon_{zz} - e_{13} E_x; \tag{6c}$$

$$\sigma_{yz} = \tilde{C}_{44} \epsilon_{yz}; \quad \sigma_{xz} = \tilde{C}_{55} \epsilon_{xz} - e_{35} E_z; \tag{6d}$$

$$\sigma_{xy} = \tilde{C}_{61} \epsilon_{xx} + \tilde{C}_{62} \epsilon_{yy} + \tilde{C}_{66} \epsilon_{xy} - e_{26} E_y. \tag{6e}$$

Standard contracted tensor notation has been used, the elastic stiffness coefficients at constant electric field

being indicated by $\tilde{C}_{pq}$ (with p and q ranging between 1 and 6), the dielectric permittivity coefficients at constant strain being represented by ϵ_{ij}, and the piezoelectric stress coefficients being indicated by e_{ip}. The above constitutive equations have been reported for the case of an orthotropic material with principal axes aligned with the structural reference system. A merely elastic material behavior can be recovered from the piezoelectric relations upon setting the coefficients e_{ip} to zero.

Classical plate theories are usually based on the kinematic assumption of a zero transverse normal strain by postulating $u_3(x,y,z)=w_0(x,y)$. However, in order to comply with the thin plate condition yielding a negligible transverse normal stress, these models employ a modified constitutive law with the following reduced coefficients (see, e.g., Fernandes and Pouget, 2001):

$$\begin{aligned} C^R_{\alpha\beta} &= \tilde{C}_{\alpha\beta} - \tilde{C}_{\beta 3}\frac{\tilde{C}_{\alpha 3}}{\tilde{C}_{33}}; \quad e^R_{ip} = e_{ip} - e_{i3}\frac{\tilde{C}_{p3}}{\tilde{C}_{33}}; \\ \varepsilon^R_{ij} &= \varepsilon_{ij} + \frac{e_{i3}\,e_{j3}}{\tilde{C}_{33}}, \end{aligned} \tag{7}$$

with $\alpha,\ \beta \in \{1,2\}$, $i,j \in \{1,2,3\}$ and $p \in \{1,\ldots,6\}$.

Irrespective of the kind of constitutive equations employed in the model, the key point in formulating an axiomatic model is to select approximations for the electrical and mechanical field variables so to consistently represent the piezoelectric interactions. As emphasized by Roccella and Gaudenzi (2005), reduced 2D models should not constrain the coupled material response in order to reproduce the relevant energetic contributions and, hence, to be confidently applicable for predicting the response of piezoelectric sensors and actuators. In the following Section, these approximations will be introduced within the notation of the GUF and a large number of 2D models will be available. Their subsequent assessment with respect to different piezoelectric interactions (i.e., direct and converse effects within extension and shear actuation modes) will permit to identify the terms of the assumptions that are responsible for the relevant energy contributions.

THE PIEZOELECTRIC GUF

The approximate structural models for the piezoelectric continuum are formulated on the basis of the irreducible Hamilton's principle in the form stated by Tiersten (1969), which in the static case reads:

$$\int_{V^k} \delta\epsilon_{ji}\,\sigma_{ij} - \delta E_i\,D_i\,\mathrm{d}V = \int_{\Gamma_t} \delta u_i\,\bar{t}_i\,\Gamma - \int_{\Gamma_q} \delta\Phi\,\bar{q}\,\Gamma. \tag{8}$$

The axiomatic assumptions for the through-thickness behavior of the generic field variable $\mathcal{U}(x,y,z)$ are expressed in GUF as:

$$\{u_x, u_y\}(x,y,z) = \sum_{s=0}^{N_u} F^u_s(z)\{\hat{u}_{xs}, \hat{u}_{ys}\}(x,y); \tag{9a}$$

$$u_z(x,y,z) = w(x,y,z) = \sum_{s=0}^{N_w} F^w_s(z)\hat{w}_s(x,y); \tag{9b}$$

$$\Phi(x,y,z) = \sum_{s=0}^{N_\Phi} F^\Phi_s(z)\hat{\Phi}_s(x,y). \tag{9c}$$

The polynomial functions $F^u_s(z)$ and $F^w_s(z)$ are the terms of the development in Taylor series, i.e.,:

$$F^u_s(z) = F^w_s(z) = z^s \tag{10}$$

with $s = 0,1,\ldots,N_u$ and $s = 0,1,\ldots,N_w$. In order to facilitate the access to prescribed values for the electrostatic potential at the top and bottom face of the plate, the polynomial functions $F^\Phi_s(z)$ are chosen by superposing higher order terms to a linear Lagrange interpolation:

$$\begin{aligned} F^\Phi_0 &= \frac{P_0 - P_1}{2}; \quad F^\Phi_1 = \frac{P_0 + P_1}{2}; \\ F^\Phi_s &= P_s - P_{s-2} \quad \text{for } s = 2,3,\ldots,N_\Phi. \end{aligned} \tag{11}$$

The basis functions P_s are Legendre polynomials defined over the non-dimensional thickness coordinate $\zeta = 2z/h$ according to:

$$P_0 = 1; \quad P_1 = \zeta; \quad P_s = \frac{1}{s}[(2s-1)\zeta P_{s-1} - (s-1)\,P_{s-2}]. \tag{12}$$

The relevant feature of this approach is that the order $N_\mathcal{U}$ of the thickness expansion for the generic field variable $\mathcal{U}$ is a free parameter of the model. By referring to the formulation in Equation (8), we have $\mathcal{U} \in \{u, w, \Phi\}$. Therefore, different models are obtained by varying the order $N_\mathcal{U}$. Models for elastic laminates will be identified by the pair $\{N_u, N_w\}$, while the triplet $\{N_u, N_w, N_\Phi\}$ will be used to identify models for piezoelectric plates. As an example, the classical Reissner–Mindlin kinematics for elastic plates can be recovered by setting $N_u = 1$ and $N_w = 0$, which corresponds to the model $\{1,0\}$. The most accurate model used in this work refers to a fourth-order expansion for all field variables and it will be indicated as $N = 4$. By adopting a sufficiently high order $N_\mathcal{U}$, this approach has proven to be capable of recovering exact 3D results even in the case of laminated structures (Ballhause et al., 2005; D'Ottavio et al., 2006, 2008). The models generally employ the full 3D constitutive laws as displayed in Equations (3)–(6). A subscript R will indicate models employing the reduced constitutive equations with the coefficients

defined in Equation (7). No shear correction factors will be used in this work.

The governing equations for the 2D models are formulated following the standard procedure (Reddy, 2004). After substituting the constitutive law and the gradient equations into Hamilton's principle, the displacement and the electrostatic potential are expressed by the axiomatic expansions given in Equation (9). A set of 2D partial differential equations is then obtained by carrying out all derivatives along z and by calculating all integrals over the cross-section. It is worth emphasizing that each contribution to the internal virtual work pertaining to each term of the polynomial approximation is formally invariant with respect to the chosen expansion orders $\{N_u, N_w, N_\Phi\}$, which leads to a particularly appealing programming simplicity (Demasi, 2008).

Navier-type Closed-form Solution

The partial differential equations governing the 2D model are solved in strong form by referring to the Navier solution (see, e.g., Reddy (2004)). Therefore, the analyses will be restricted to rectangular plates of dimension $a \times b$ and constant thickness h made of orthotropic materials and with simply–supported edges for which the following conditions hold:

$$\tilde{C}_{45} = \tilde{C}_{16} = \tilde{C}_{26} = \tilde{C}_{36} = 0; \tag{13a}$$

$$u_x(x, y = 0) = u_x(x, y = b) = 0; \tag{13b}$$

$$u_y(x = 0, y) = u_y(x = a, y) = 0; \tag{13c}$$

$$w(x = 0, y) = w(x = a, y) = w(x, y = 0) = w(x, y = b) = 0 \tag{13d}$$

$$\sigma_{xx}(x = 0, y) = \sigma_{xx}(x = a, y) = 0 \tag{13e}$$

$$\sigma_{yy}(x, y = 0) = \sigma_{yy}(x, y = b) = 0. \tag{13f}$$

The Navier solution is expressed in terms of trigonometric functions which exactly meet all boundary conditions in the following manner (Batra and Aimmanee, 2003):

$$\hat{u}_{x\,s}(x, y) = \sum_{m_x=0}^{\infty} \sum_{m_y=0}^{\infty} U_{x\,s\,m_x m_y} \cos\left(\frac{m_x \pi x}{a}\right) \sin\left(\frac{m_y \pi y}{b}\right); \tag{14a}$$

$$\hat{u}_{y\,s}(x, y) = \sum_{m_x=0}^{\infty} \sum_{m_y=0}^{\infty} U_{y\,s\,m_x m_y} \sin\left(\frac{m_x \pi x}{a}\right) \cos\left(\frac{m_y \pi y}{b}\right); \tag{14b}$$

$$\hat{w}_s(x, y) = \sum_{m_x=0}^{\infty} \sum_{m_y=0}^{\infty} W_{s\,m_x m_y} \sin\left(\frac{m_x \pi x}{a}\right) \sin\left(\frac{m_y \pi y}{b}\right). \tag{14c}$$

The admissible electrical boundary conditions and the corresponding Navier solution depend on the polarization scheme:

- Thickness (z-axis) polarization:

$$\Phi(x = 0, y) = \Phi(x = a, y) = \Phi(x, y = 0) = \Phi(x, y = b) = 0; \tag{15a}$$

$$\hat{\Phi}_s(x,y) = \sum_{m_x=0}^{\infty} \sum_{m_y=0}^{\infty} V_{s\,m_x m_y} \sin\left(\frac{m_x \pi x}{a}\right) \sin\left(\frac{m_y \pi y}{b}\right). \tag{15b}$$

- In-plane (x-axis) polarization:

$$\Phi(x, y = 0) = \Phi(x, y = b) = 0; \quad D_x(x = 0, y) = D_x(x = a, y) = 0. \tag{16a}$$

$$\hat{\Phi}_s(x, y) = \sum_{m_x=0}^{\infty} \sum_{m_y=0}^{\infty} V_{s\,m_x m_y} \cos\left(\frac{m_x \pi x}{a}\right) \sin\left(\frac{m_y \pi y}{b}\right). \tag{16b}$$

In this work, we consider only the static response of the fundamental flexural mode by setting always $m_x = m_y = 1$. The response to more general loading distributions requires the use of the complete series solution given in Equations (14), (15b), and (16b) (see, e.g., Carrera et al., 2007). If free-vibration analyses are addressed, the vibration modes associated to different values for m_x and m_y should be carefully chosen (Batra and Aimmanee, 2003).

LINEAR ELASTIC PLATES

Preliminary numerical investigations are dedicated to the purely elastic response of a homogeneous and isotropic square plate in bending. The plate thickness is $h = 1$ mm and different aspect ratios $S = a/h$ are considered. The employed material data correspond to those of a typical Aluminum alloy (Al 2024) with Young's modulus $E = 73$ GPa and Poisson's ratio $\nu = 0.34$. The plate is loaded on its top face by a distributed pressure:

$$p\left(x, y, z = \frac{h}{2}\right) = p_0 \sin\left(\frac{\pi x}{a}\right) \sin\left(\frac{\pi y}{b}\right). \tag{17}$$

The results for several reduced models are reported in Table 1 in terms of the non-dimensional deflection at the plate mid-point:

$$\bar{w}(z = 0) = \frac{100E}{p_0 h^3 S^4} w(x = 0, y = 0, z = 0). \tag{18}$$

All 2D models employ the full 3D constitutive relation and are labeled by their kinematics defined by the

Table 1. Bending of a simply supported, isotropic plate made of Al 2024: non-dimensional deflections $\bar{w}(z=0)$ for different models $\{N_u, N_w\}$ employing the full 3D constitutive law.

S	3D	{1,0}	{1,1}	{1,2}	{2,1}	{2,2}	{2,3}	{3,2}
10	2.8655	2.1367	2.1367	2.8469	2.1367	2.8469	2.8469	2.8655
100	2.7252	2.0023	2.0023	2.7250	2.0023	2.7250	2.7250	2.7252
1000	2.7238	2.0009	2.0009	2.7238	2.0009	2.7238	2.7238	2.7238

Table 2. Non-dimensional deflection $\bar{w}(z=0)$ and percentage error with respect to exact solution for the Reissner–Mindlin kinematics {1,0} with 3D and 2D (subscript R) constitutive law: selected combinations of aspect ratios $S=a/h$ and Poisson's ratios ν.

S	Exact	$\bar{w}_{\{1,0\}}$	Δ(%)	$\bar{w}_{\{1,0\}R}$	Δ_R(%)
		$\nu=0.05$			
4	3.8389	3.7285	2.88	3.7370	2.65
10	3.1970	3.1700	0.84	3.1785	0.58
1000	3.0721	3.0636	0.28	3.0721	0.00
		$\nu=0.45$			
4	3.3561	1.7302	48.45	3.3744	0.55
10	2.6023	0.9589	63.15	2.6031	0.03
1000	2.4562	0.8120	66.94	2.4562	0.00

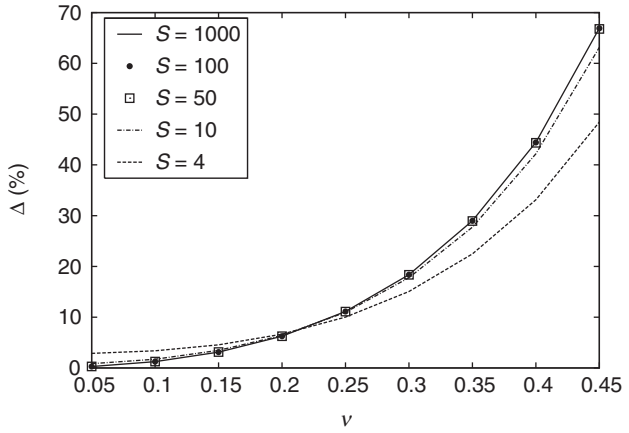

Figure 1. Percentage error on the transverse deflection for the model based on Reissner–Mindlin kinematics {1,0} and full 3D constitutive law: influence of Poisson's ratio ν and aspect ratio $S=a/h$.

pair $\{N_u, N_w\}$. The exact 3D solution has been obtained according to Demasi (2006). The results in Table 1 indicate that an excessively stiff response is found for all models with $N_w < 2$ when the full 3D constitutive law is used. The constant transverse normal strain ϵ_{zz} described by this kinematics does not match the linear contributions of the bending strains ϵ_{xx} and ϵ_{yy} in the definition of the bending stresses σ_{xx} and σ_{yy} given in Equations (4a) and (4b). This mechanism promotes the so-called Poisson locking phenomenon (Büchter et al., 1994; Carrera and Brischetto, 2008a,b). Table 1 shows that the exact solution for thin plates in bending can be recovered by the model $\{1,2\}$ (see also Paumier and Raoult, 1997).

In thick plates (i.e., $S \leq 10$), the bending deformation comes along with transverse shear strain. In order to capture this effect, a refined description of the in-plane displacement is required. The quadratic approximation for the transverse deflection is still necessary for avoiding Poisson locking. Both requirements are met in the model $\{3,2\}$, which leads to a quadratic variation of the transverse shear strain along the cross section. Table 1 shows that this model correctly recovers the exact solution for all thickness ranges. The importance of a parabolic distribution of the transverse shear stresses σ_{xz} and σ_{yz} is highlighted in Table 1 by the superior accuracy of the $\{3,2\}$ kinematics with respect to the model $\{2,3\}$, which is in turn characterized by a quadratic behavior of the bending stresses σ_{xx} and σ_{yy}.

In order to emphasize the role of Poisson's ratio ν within this peculiar locking phenomenon, the influence of this material parameter on the accuracy of classical plate kinematics has been detailed out. Table 2 and Figure 1 report the errors produced when the Reissner–Mindlin kinematics $\{N_u,\ N_w\}=\{1,0\}$ is used in conjunction with a full 3D constitutive law. The results in Table 2 show that this kinematics requires the modified coefficients defined in Equation (7) in order to annihilate the large errors of Poisson locking. As shown in Figure 1, the error depends quadratically on the value of Poisson's ratio ν. By investigating the role of aspect ratio on Poisson locking, Figure 1 shows that the curves related to $S=50$, 100, and 1000 coincide, i.e. the error is not affected by the geometric parameter S if the plate is thin enough. For small aspect ratios (i.e., $S \leq 10$), the errors due to low-order kinematic assumptions gain relevance and represent the dominant error source for small values of Poisson's ratio. Furthermore, for increasing Poisson's ratio ν, the error for thick plates is shown to grow slower in comparison to the thin plate case. These results lead to the conclusion that Poisson locking is a material-dependent issue and not a geometry-dependent error source.

PIEZOELECTRIC PLATE WORKING IN 31-MODE

We consider a square piezoelectric plate of side a and thickness $h=1$ mm made of PZT-4 polarized along the thickness direction. Sensor and actuator configurations

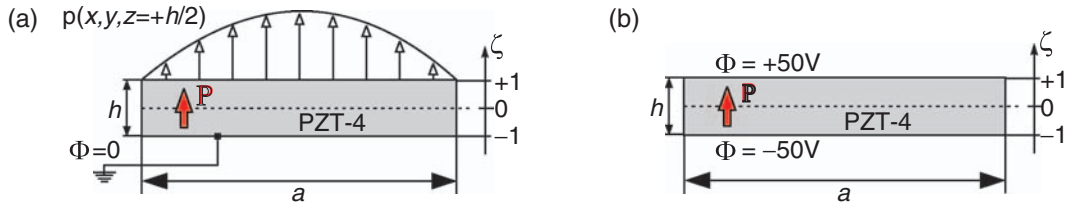

(c)

$E_1 = E_2$	81.3	[GPa]	$e_{31} = e_{32}$	−5.20	$\left[\frac{C}{m^2}\right]$
E_3	64.5	[GPa]	e_{33}	15.08	$\left[\frac{C}{m^2}\right]$
$\nu_{13} = \nu_{23}$	0.432	[–]	$e_{15} = e_{24}$	12.72	$\left[\frac{C}{m^2}\right]$
ν_{12}	0.329	[–]	$\varepsilon_{11} = \varepsilon_{22}$	$1475\varepsilon_0$	$\left[\frac{C}{Vm}\right]$
$G_{13} = G_{23}$	25.6	[GPa]	ε_{33}	$1300\varepsilon_0$	$\left[\frac{C}{Vm}\right]$
G_{12}	30.6	[GPa]	ρ	7500	$\left[\frac{kg}{m^3}\right]$

Figure 2. *Piezoelectric plate working in 31-mode (transverse extension): schematic of sensor and actuator configurations (top) and material data for PZT-4 poled along the transverse z-axis (bottom): (a) Sensor configuration; (b) Actuator configuration; (c) Material data for transverse polarized PZT-4 ($\varepsilon_0 = 8.85410^{-12}$ C/Vm).*

of a homogeneous PZT-4 plate are analyzed as shown in Figure 2. In the sensor case (Figure 2(a)), the bottom face of the plate is grounded $\Phi(\zeta = -1) = 0$ and the following pressure load is prescribed on the top face:

$$p\left(x, y, z = \frac{h}{2}\right) = p_0 \sin\left(\frac{\pi x}{a}\right) \sin\left(\frac{\pi y}{b}\right), \tag{19}$$

with the load amplitude $p_0 = 1$ MPa. In the actuator configuration (Figure 2(b)), no mechanical loading is present and the deformation is induced by an applied electric field $\bar{E}_{z0}$. For this, the electrostatic potential on the top and bottom surfaces of the plate is prescribed according to:

$$\begin{aligned} \Phi\left(x, y, z = \frac{h}{2}\right) &= \frac{\Phi_0}{2} \sin\frac{\pi x}{a} \sin\frac{\pi y}{a}; \\ \Phi\left(x, y, z = -\frac{h}{2}\right) &= -\frac{\Phi_0}{2} \sin\frac{\pi x}{a} \sin\frac{\pi y}{a}. \end{aligned} \tag{20}$$

The prescribed potential level is $\Phi_0 = 100$ V and the resulting electric field is $\bar{E}_{z0} = 100$ V/mm.

Based on previous results obtained for piezoelectric laminates (Ballhause et al., 2005), in the following the solution of the most accurate model $N = 4$ will be considered as the reference solution.

Sensor Configuration

The sensor response is characterized by a bending deformation of the plate by virtue of the applied pressure load. Accordingly, the considered response parameters will be made non-dimensional in the following manner:

$$\begin{aligned} \bar{w} &= \frac{100\,\tilde{C}_{11}}{p_0 a\, S^3}\, w; \quad \bar{\Phi} = \frac{e_{31}}{p_0\, a^2}\, \Phi. \\ \bar{\sigma}_{xx} &= \frac{1}{p_0\, S^2}\, \sigma_{xx}; \quad \bar{\sigma}_{xz} = \frac{1}{p_0\, S}\, \sigma_{xz}. \end{aligned} \tag{21}$$

The stress components are computed directly from the constitutive relations given in Equation (4).

Figure 3 reports the evolution of the non-dimensional parameters $\bar{w}$ and $\bar{\Phi}$ evaluated at the plate center $\zeta = 2z/h = 0$ for varying aspect ratio S. The results show that an at least quadratic approximation for the electrostatic potential is necessary to capture the piezoelectric interaction. Models with $N_\Phi = 1$ (i.e., the models $\{1, 1, 1\}$ and $\{1, 2, 1\}$) predict an incorrect deflection that is larger than that of their counterparts with $N_\Phi = 2$ (i.e., the models $\{1, 1, 2\}$ and $\{1, 2, 2\}$, respectively). This occurs because models with $N_\Phi < 2$ fail to represent the electrostatic potential that is induced by the bending strains through the direct piezoelectric effect (Equations (3) and (4)). An at least linear electric field, i.e., an at least quadratic electrostatic potential, is necessary to match the linear bending strains and, hence, to represent the amount of deformation energy that is converted into electric energy by the piezoelectric sensor. The piezoelectric coupling is thus responsible for an augmentation of the apparent stiffness of the piezoelectric plate. The results in Figure 3 indicate that the error associated to the missing piezoelectric stiffness is not substantially affected by the slenderness of the piezoelectric plate. In fact, the need for a quadratic approximation for the electrostatic potential is dictated by the

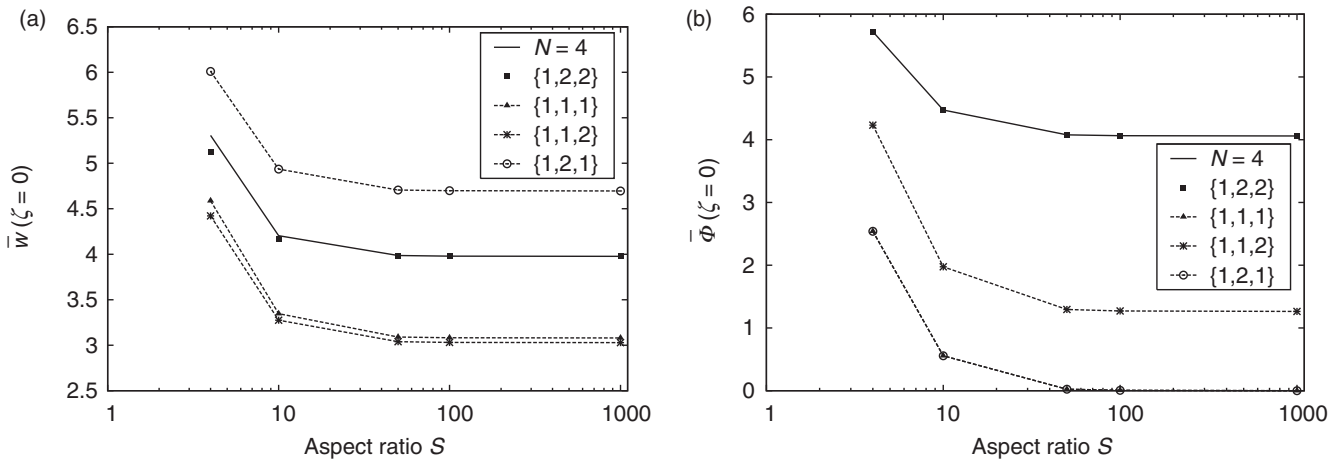

Figure 3. *Piezoelectric sensor plate in 31-mode: non-dimensional global electromechanical response at the plate center for different aspect ratio $S = a/h$ ($h =$ constant): (a) Normalized deflection $\bar{w}(\zeta = 0)$; (b) Normalized electric potential $\bar{\Phi}$ $(\zeta = 0)$.*

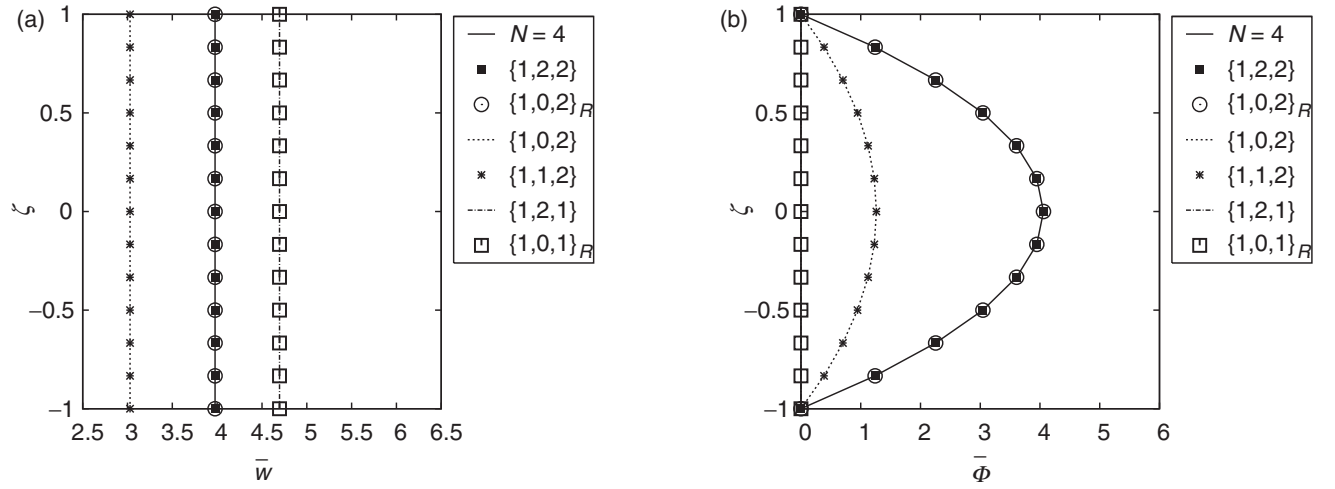

Figure 4. *Thin ($S = 1000$) piezoelectric sensor plate in 31-mode: through-thickness distribution of the transverse deflection (left) and electrostatic potential (right) for selected low-order models: (a) Normalized deflection $\bar{w}$; (b) Normalized electric potential $\bar{\Phi}$.*

piezoelectric coupling and, hence, it does not depend on the geometric properties of the plate. Furthermore, the results obtained with the models $\{1, 1, 1\}$ and $\{1, 1, 2\}$ demonstrate that an at least quadratic distribution of the transverse displacement is necessary when the full 3D constitutive law is employed. This extends the validity of the remarks concerning Poisson locking (section 'Linear Elastic Plates') to piezoelectric plates.

Figure 4 reports the through-thickness distributions of the non-dimensional response parameters $\bar{w}$ and $\bar{\Phi}$ obtained for a quite thin plate ($S = 1000$) by several low-order models with $N_u = 1$. The reference solution ($N = 4$) yields a parabolic and symmetric distribution of the electrostatic potential, whose value is zero at the top surface: $\bar{\Phi}(\zeta = 1) = 0$. Models with $N_w < 2$ and full 3D constitutive law suffer Poisson locking and possess a spurious additional stiffness. On the other hand, models with $N_\Phi < 2$ are not capable to capture the induced electric field and predict larger deformations because of the missing piezoelectric stiffness. Furthermore, no difference can be noted between the model $\{1, 0, 1\}_R$ (respectively $\{1, 0, 2\}_R$) and the model $\{1, 2, 1\}$ (respectively $\{1, 2, 2\}$). The same behavior is thus found for models exploiting the reduced constitutive coefficients with $N_w = 0$ and those using the full 3D constitutive law with $N_w = 2$.

The local response is reported in Figure 5 in terms of through-thickness distributions of the non-dimensional stresses $\bar{\sigma}_{xx}$ and $\bar{\sigma}_{xz}$. The considered low-order models (i.e., models with $N_u = 1$) represent accurately the primary bending stress σ_{xx}, see Figure 5(a). However, Figure 5(b) shows that they yield only an estimate of

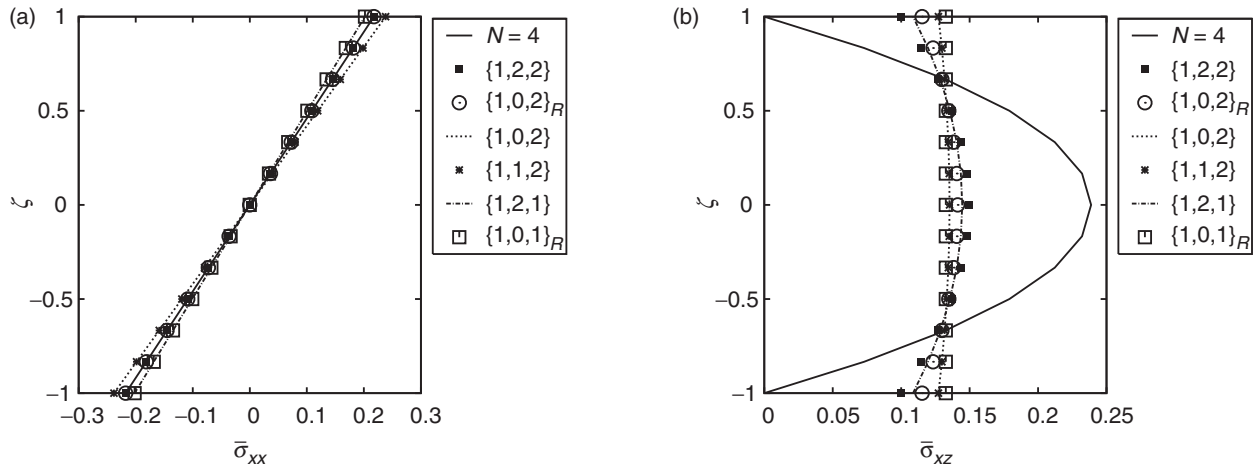

Figure 5. *Thin (S = 1000) piezoelectric sensor plate in 31-mode: through-thickness distribution of the non-dimensional in-plane and transverse shear stresses for selected low-order models: (a) In-plane stress $\bar{\sigma}_{xx}$; (b) Transverse shear stress $\bar{\sigma}_{xz}$.*

the average transverse shear deformation because the linear assumption for the in-plane displacement ($N_u = 1$) does not capture the quadratic distribution of the transverse shear strain. It may be noted that a (weak) quadratic dependency of the transverse shear deformation is introduced by taking $N_w \geq 2$ and/or $N_\Phi \geq 2$. In the former case, the quadratic term is due to the definition of the transverse shear strains $\gamma_{xz} = u_{,z} + w_{,x}$. In the second case, the quadratic assumption for the electric potential enters in the transverse shear stress *via* the piezoelectric coefficient e_{15}, as given in Equation (4d). Nevertheless, both terms are of second-order compared with the parabolic distribution obtained by using a higher-order approximation for the in-plane displacement.

Figure 6 reports the through-thickness distributions of $\bar{w}$ and $\bar{\Phi}$ for a thick sensor plate ($S = 4$) and selected models with low-order ($N_u = 1$) and higher-order ($N_u > 1$) kinematic approximations. The reference solution obtained with $N = 4$ shows that the electrostatic potential has still a parabolic distribution. Furthermore, a certain asymmetry is introduced by the 3D effects and the asymmetric loading. Hence, a non-zero value for Φ is obtained at the top surface of the piezoceramic plate. The results in Figure 6 indicate that the 3D effects in the thick plate enhance the discrepancies between different models. An accurate prediction of the response of a thick plate demands the use of refined models with higher-order kinematic assumptions. Figure 6(c) suggests that the model $\{3, 2, 2\}$ is capable of capturing the principal deformation patterns over the cross-section. This is attributed to the quadratic description of the transverse shear strain as well as to the representation of transverse normal deformation. In particular, it is worth to remark the inaccuracies introduced by the use of the hypothesis $\sigma_{zz} = 0$ and the consequent reduced constitutive law. Due to the plate thickness, transverse normal deformation effects are important and affect the piezoelectric coupling as well. Figure 6(d) shows that models with $N_w = 0$ and employing the reduced constitutive coefficients yield an inaccurate prediction of the voltage level at the top electrode of the sensor. Finally, note that the considerations made for the thin plate case concerning Poisson locking hold for the thick plate as well.

The stress response in the thick ($S = 4$) sensor plate in 31-mode is illustrated in Figure 7. The discrepancies between low-order models (top of Figure 7) and higher-order models (bottom of Figure 7) are negligible as far as the primary bending stress σ_{xx} is concerned. However, if an accurate evaluation of the transverse shear stress is required, an at least cubic assumption for the in-plane displacement should be employed. Figure 7(b) and (d) shows that models with $N_u < 3$ can only provide an estimate of the average transverse shear deformation and that they violate the stress-free condition at the outer surfaces of the plate. It is finally remarked that using the reduced constitutive law does not degrade the accuracy of the calculated stress components.

Actuator Configuration

The application of an electric field along the thickness of transversely polarized piezoceramics has as primary effect a membrane deformation. Frequently used piezoelectric actuators are bender elements that are implemented by combining two actuators with opposite resulting in-plane deformation (see, e.g., Chao and Shen (2007); Fernandes and Pouget (2003); Vel and Batra (2001a)). With reference to the schematic of Figure 2(b), the applied voltage produces a contraction of the plate (i.e., $\hat{u} = \hat{v} < 0$) *via* the e_{31} and e_{32} coefficients given in Figure 2(c)). As a secondary

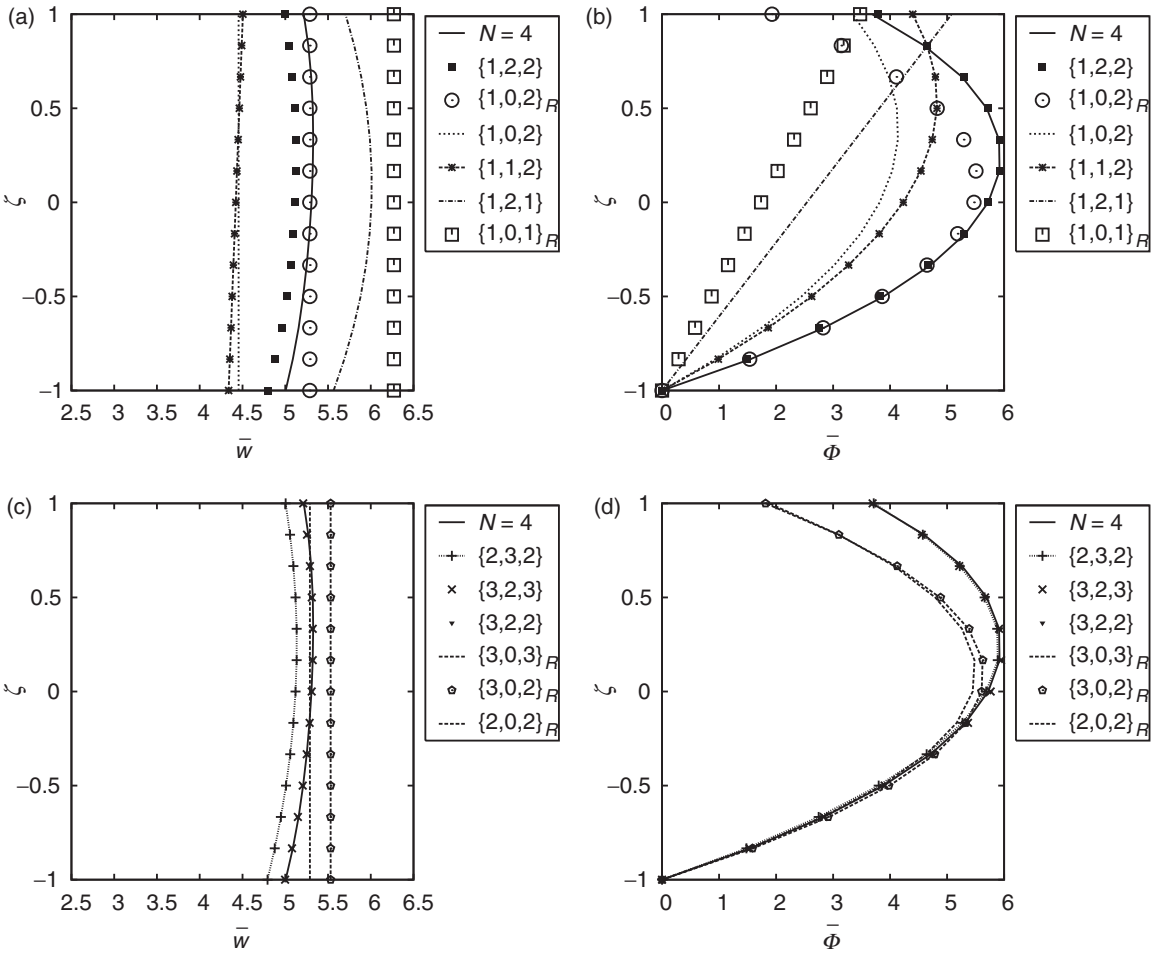

Figure 6. *Thick (S = 4) piezoelectric sensor plate working in 31-mode: through-thickness distribution of the non-dimensional transverse deflection (left) and electrostatic potential (right) for selected low-order ($N_u = 1$, top) and higher-order ($N_u > 1$, bottom) models: (a) Normalized deflection $\bar{w}$; (b) Normalized electric potential $\bar{\Phi}$; (c) Normalized deflection $\bar{w}$; (d) Normalized electric potential $\bar{\Phi}$.*

effect, a non-Poisson transverse deformation arises due to the piezoelectric coefficient e_{33}. For the considered single actuator, the following non-dimensional response parameters will be considered:

$$\bar{u} = \frac{\tilde{C}_{11}}{e_{31} E_{z0}\, a}\, u_x; \quad \bar{w} = \frac{\tilde{C}_{11}}{e_{31}\Phi_0}\, w; \quad \bar{\sigma}_{xx} = \frac{1}{e_{31}\, E_{z0}}\, \sigma_{xx};$$
$$\bar{\sigma}_{xz} = \frac{a}{e_{31}\, \Phi_0}\, \sigma_{xz}; \quad \bar{\Phi} = \frac{1}{\Phi_0}\, \Phi. \tag{22}$$

The reference value of the transverse electric field is $E_{z0} = \Phi_0/h$ and $\Phi_0 = 100\,\mathrm{V}$, see Figure 2(b). The stress components are calculated through the constitutive Equation (4).

Through-thickness distributions of the non-dimensional response for a thin actuator ($S = 1000$) are reported in Figures 8 and 9. The electrical and mechanical response result to be decoupled since the distribution of the electrostatic potential is independent of the employed kinematic model. A linear approximation for the electrostatic potential is sufficient for correctly representing the actuating electric field, see Figure 8(c). The actuation authority (i.e., the membrane deformation) is well captured by a constant assumption for the in-plane displacement components , i.e., by models with $N_u = 0$. In this case, and if the full 3D constitutive law is employed, an at least linear assumption for the transverse deflection w is necessary to prevent the spurious Poisson locking: the model $\{0, 0, 1\}$ has a spuriously increased stiffness and leads to errors in the actuation authority as high as 70%. As shown by the results of the model $\{0, 0, 1\}_R$, the modified constitutive law is an effective means for eliminating the Poisson locking and for recovering the correct membrane deformation of the piezoelectric actuator, see Figures 8(a),(b) and 9(a). However, models with $N_u = 0$ prove useless for a prediction of the transverse shear stress, see Figure 9(b).

The non-dimensional response in a thick ($S = 4$) piezoelectric actuator in 31-mode is given in Figures 10

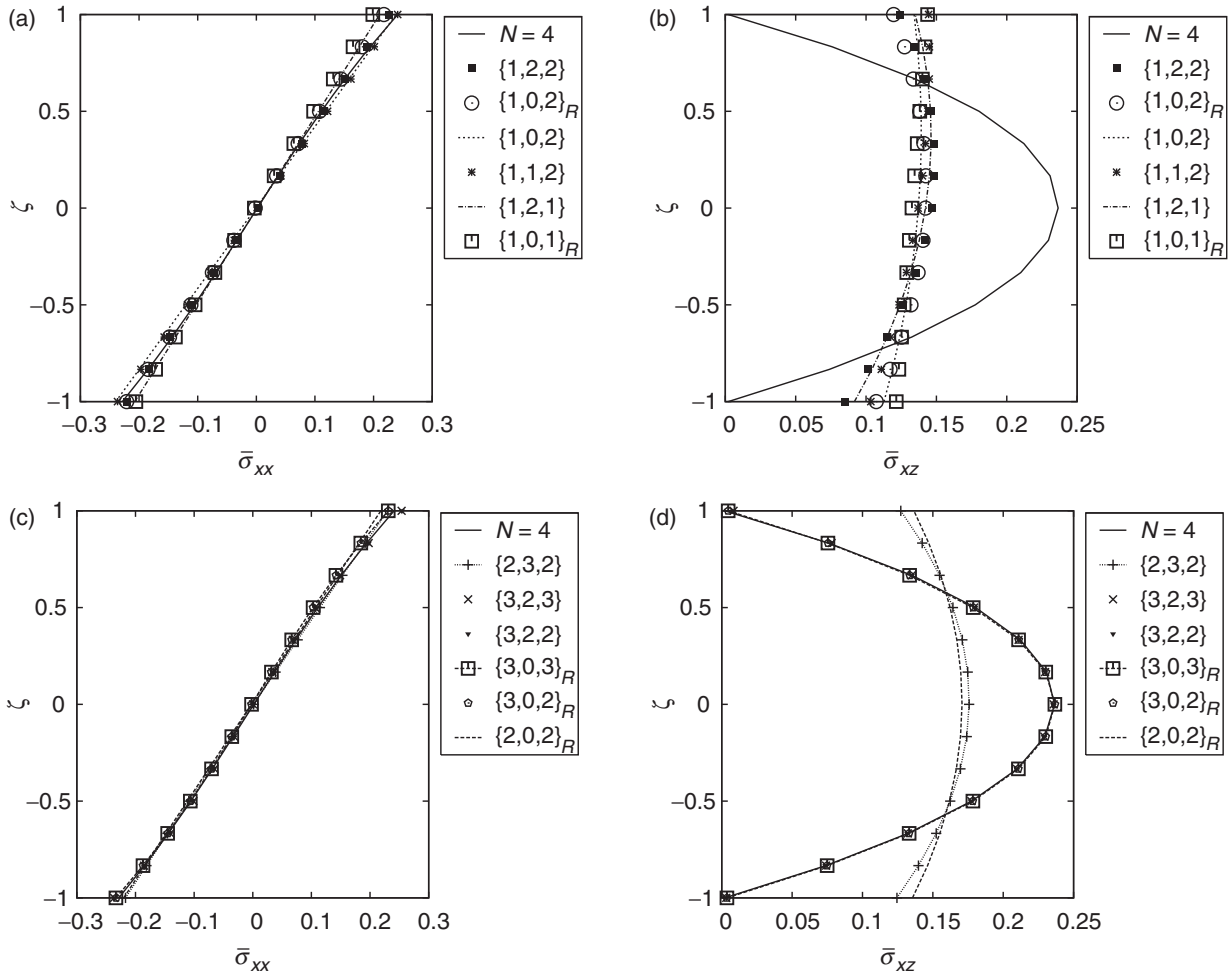

Figure 7. *Thick (S = 4) piezoelectric sensor plate working in 31-mode: through-thickness distribution of the non-dimensional in-plane and transverse shear stresses obtained with several low-order ($N_u = 1$, top) and higher-order ($N_u > 1$ bottom) models: (a) In-plane direct $\bar{\sigma}_{xx}$; (b) Transverse shear stress $\bar{\sigma}_{xz}$; (c) In-plane direct stress $\bar{\sigma}_{xx}$; (d) Transverse shear stress $\bar{\sigma}_{xx}$.*

and 11. Due to the thickness of the patch, the actuating electric field is slightly non-uniform and the electrostatic potential marginally deviates from the linear behavior. The antisymmetric boundary conditions on the applied voltage calls for an odd polynomial order for the electrostatic potential. Hence a cubic approximation $N_\Phi = 3$ exactly represents the non-linear through-thickness distribution, but a linear assumption is an excellent approximation, see Figure 10(c). Note that the kinematic assumptions do not affect the distribution of the electrostatic potential.

The mechanical response of the thick actuator is affected by 3D effects and is characterized by a warping of the cross-section, see Figure 10(a). This comes along with slightly non-uniform in-plane (membrane) and transverse shear stresses, as illustrated in Figure 11. Models with $N_u > 1$ are thus necessary. However, models with $N_u = 0$ provide a good estimate of the mean actuation. Table 3 compares the mean non-dimensional displacement $\bar{u}$ obtained with selected models. The mean actuation authority for models with a non-linear distribution has been evaluated as the center of gravity of a parabolic distribution. If the full 3D constitutive law is employed, an at least linear assumption for the transverse deflection is necessary to avoid Poisson locking. The model $\{2, 1, 1\}$ provides good results for the displacement field, see Figure 10(a) and (b), but it predicts an incorrect distribution of the membrane stress σ_{xx}, as shown in Figure 11(a). If the assumption $N_u = 2$ is completed by higher order (cubic) approximations only for the transverse displacement w, only marginal improvements are achieved for the membrane stress. In fact, Figure 11(a) shows that a higher accuracy in the stress response requires the use of higher order assumptions for both the transverse displacement and the actuating electric field. Since $\epsilon_{zz} = w_{,z}$ and $E_z = -\Phi_{,z}$ introduce into the definition of the membrane stress the same dependency on the thickness coordinate z, the same third-order approximation $N_w = N_\Phi = 3$ can be used

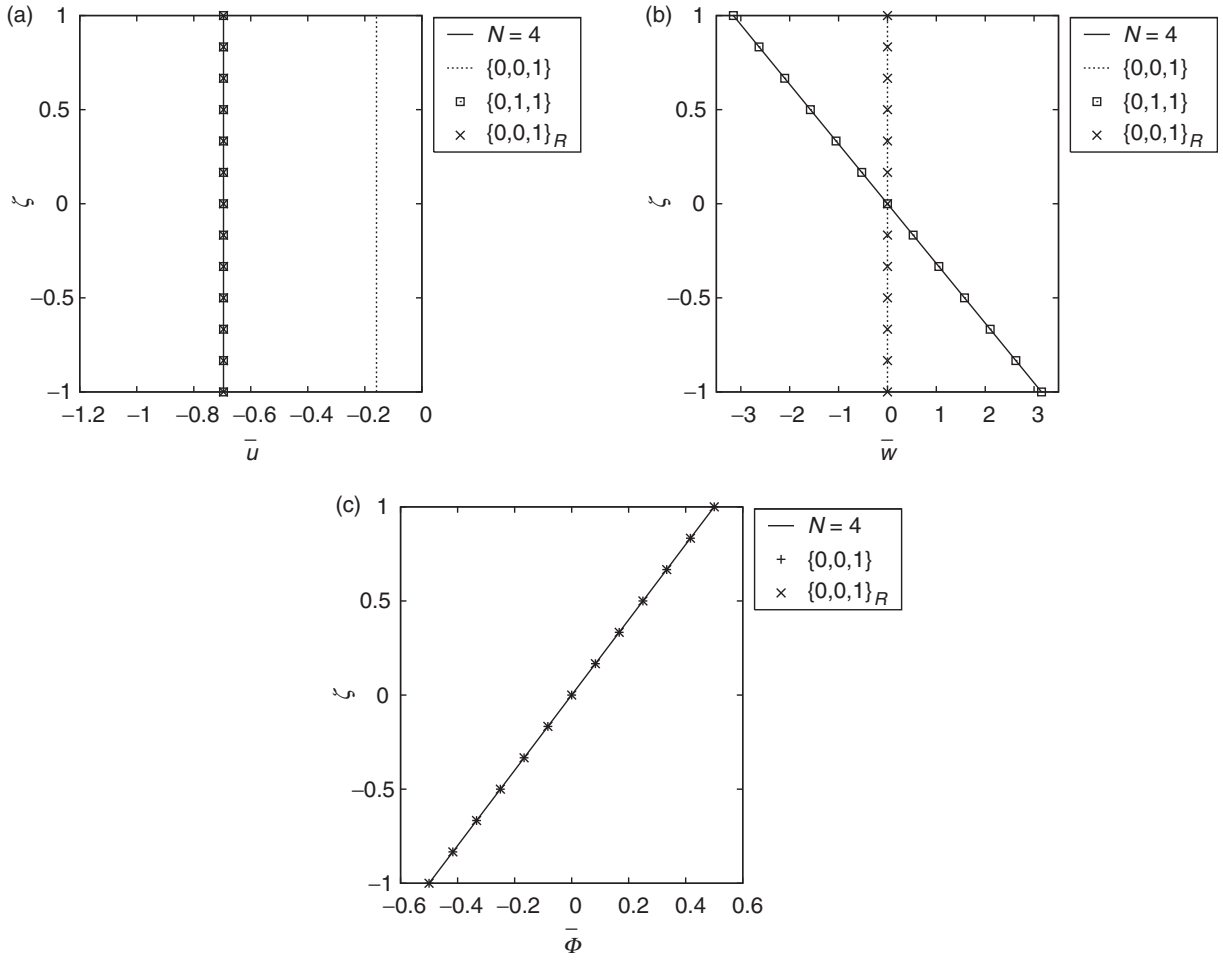

Figure 8. *Thin (S = 1000) actuator working in 31-mode: through-thickness distribution of the membrane displacement (top left), transverse deflection (top right) and electrostatic potential (bottom) for selected* 2D *models: (a) Normalized displacement $\bar{u}$; (b) Normalized diflection $\bar{w}$; (c) Normalized electric potential $\bar{\Phi}$.*

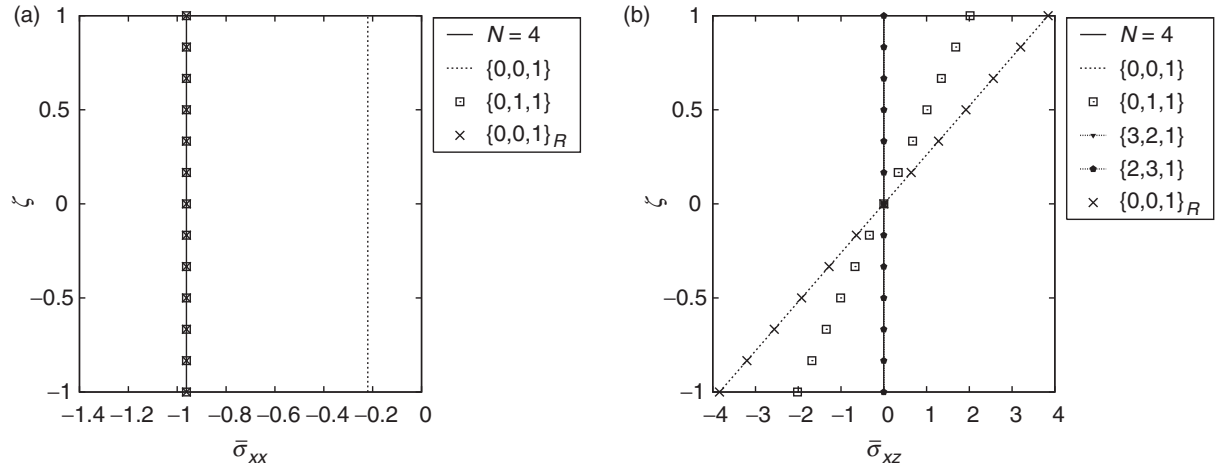

Figure 9. *Thin (S = 1000) piezoelectric actuator in 31-mode: Through-thickness distributions of the non-dimensional in-plane and transverse shear stresses: (a) In-plane stress $\bar{\sigma}_{xx}$; (b) Transverse shear stress $\bar{\sigma}_{xz}$.*

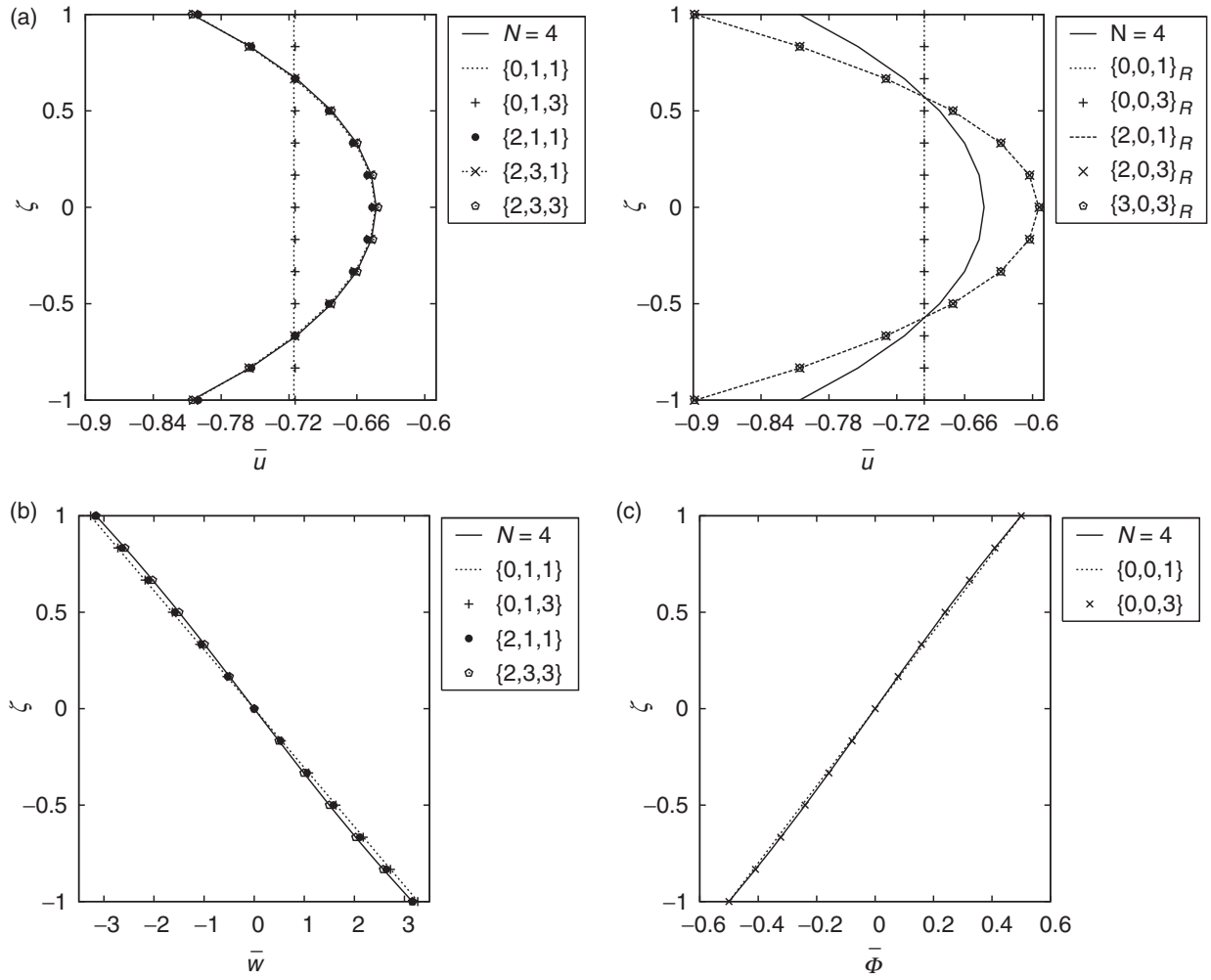

Figure 10. *Thick (S = 4) piezoelectric actuator in 31-mode: through-thickness distribution of the in-plane displacement (top), the transverse deflection (bottom left) and electrostatic potential (bottom right): (a) Normalized displacement $\bar{u}$: models with* 3D *constitutive law (left) and with reduced constitutive coefficients (right); (b) Normalized deflection $\bar{w}$; (c) Normalized electric potential $\bar{\Phi}$.*

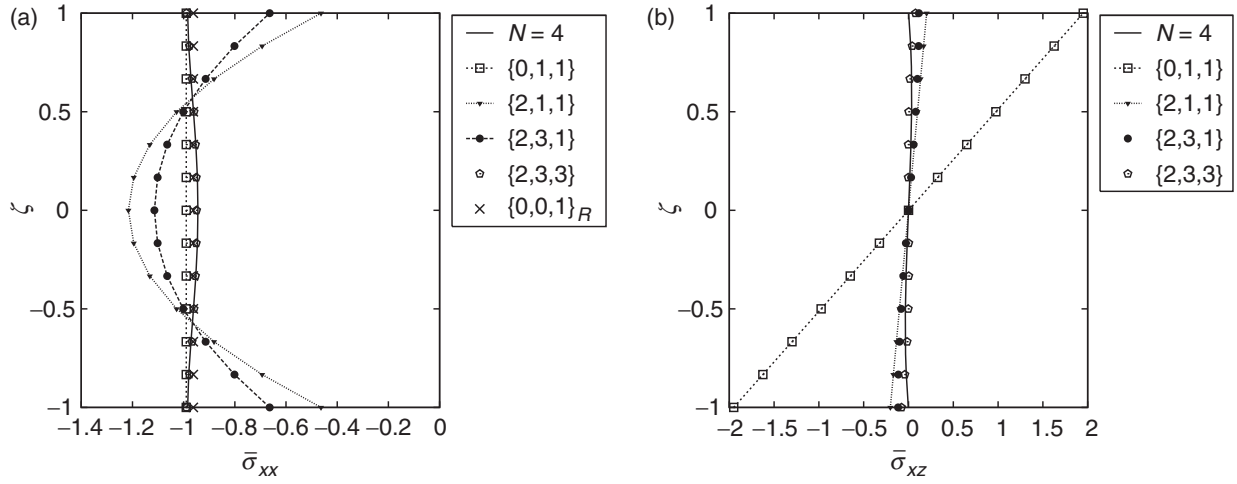

Figure 11. *Thick (S = 4) piezoelectric actuator in 31-mode: Through-thickness distributions of the non-dimensional in-plane and transverse shear stresses: (a) In-plane stress $\bar{\sigma}_{xx}$; (b) Transverse shear stress $\bar{\sigma}_{xz}$.*

for both field variables. Hence, higher order approximations for $\Phi(z)$ play an important role in the piezoelectric coupling even if they are not necessary for the representation of the actuating electric field as illustrated in Figure 10(c). As an alternative, models with $N_w = 0$ and based on the reduced constitutive law can be used for estimating the mean actuation authority and the membrane stress, see Table 3 and Figure 11(a). Finally, the right-hand side of Figure 10(a) shows that models with higher order in-plane kinematics and reduced constitutive coefficients lead to inaccuracies of the order of ~10% in the representation of the warping.

PIEZOELECTRIC PLATE WORKING IN 15-MODE

The axiomatic assumptions are assessed for models of simply supported piezoelectric plates exploiting the shear actuation mechanism. Square piezoelectric sensor and actuator plates of constant thickness $h = 1$ mm and with the poling direction aligned with the in-plane first axis (i.e., the x-axis) are considered according to the schematic in Figure 12. The material parameters of the in-plane polarized PZT-4 are reported in Figure 12(c) and have been obtained from those of the transversely polarized piezoceramic upon a double tensorial transformation that rotates the polarization axes (Benjeddou et al., 1997).

Table 3. Actuation authority of a thick ($S = 4$) piezoelectric actuator: mean non-dimensional in-plane displacement for different 2D models.

$\{N_u, N_w, N_\Phi\}$	$\{4,4,4\}$	$\{0,0,1\}$	$\{2,1,3\}$	$\{3,1,1\}$
mean $\bar{u}$	−0.708	−0.159	−0.707	−0.708
$\{N_u, N_w, N_\Phi\}$	$\{2,3,3\}$	$\{0,0,1\}_R$	$\{2,0,3\}_R$	$\{3,0,3\}_R$
mean $\bar{u}$	−0.707	−0.696	−0.716	−0.716

Results previously obtained for piezoelectric laminates (D'Ottavio et al., 2008) indicate that the solution of the most accurate model $N = 4$ can be considered as the reference solution.

Sensor Configuration

The bending response for the piezoelectric sensor of Figure 12(a) and subjected to a lateral pressure load is made non-dimensional according to

$$\bar{u} = \frac{\tilde{C}_{55}}{p_0 a S^2} u; \quad \bar{w} = \frac{100\tilde{C}_{55}}{p_0 a S^3} w; \quad \bar{\Phi} = \frac{e_{35}}{p_0 a} \Phi; \\ \bar{\sigma}_{xx} = \frac{1}{p_0 S^2} \sigma_{xx}; \quad \bar{\sigma}_{xz} = \frac{1}{p_0 S} \sigma_{xz}. \tag{23}$$

The non-dimensional response of a thin ($S = 1000$) sensor working in shear mode is reported in Figures 13 and 14. One observes the typical bending response, in which a linear in-plane displacement and direct stress are accompanied by a quadratic transverse deflection and shear stress (Figures 13(a), (b) and 14). The presence of Poisson locking is confirmed whenever $N_w < 2$ is used in conjunction with the full 3D constitutive law: Figures 13(a) and 14(a) show that the model $\{1,0,1\}$ underestimates the plate deformation being excessively stiff due to Poisson locking. Observing the results of the model $\{1,0,1\}$ in Figure 13(c), one notes that Poisson locking yields a larger value of the sensed voltage at the top electrode. Hence, in contrast to the piezoelectric plate working in 31 mode, in shear-actuated plates the underestimated deflection due to Poisson locking comes along with a larger value of the sensed potential.

The response of thick ($S = 4$) sensors working in shear mode, Figures 15 and 16, is affected by the 3D effects

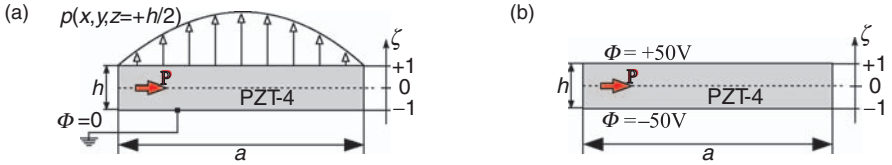

(c)

E_1	64.5	[GPa]	$e_{12} = e_{13}$	−5.20	$\left[\frac{C}{m^2}\right]$
$E_2 = E_3$	81.3	[GPa]	e_{11}	15.08	$\left[\frac{C}{m^2}\right]$
$\nu_{12} = \nu_{13}$	0.432	[–]	$e_{26} = e_{35}$	12.72	$\left[\frac{C}{m^2}\right]$
ν_{23}	0.329	[–]	ε_{11}	$1300\,\varepsilon_0$	$\left[\frac{C}{Vm}\right]$
$G_{12} = G_{13}$	25.6	[GPa]	$\varepsilon_{22} = \varepsilon_{33}$	$1475\varepsilon_0$	$\left[\frac{C}{Vm}\right]$
G_{23}	30.6	[GPa]	ρ	7500	$\left[\frac{kg}{m^3}\right]$

Figure 12. *Piezoelectric plate working in 15-mode (shear mode): schematic of sensor and actuator configurations (top) and employed material data for PZT-4 (bottom). The polarization vector* ***P*** *is taken parallel to the x-axis: (a) Sensor configuration; (b) Actuator configuration; (c) Material data for PZT-4 poled along x-axis ($\epsilon_0 = 8.854\ 10^{-12}$ C/Vm).*

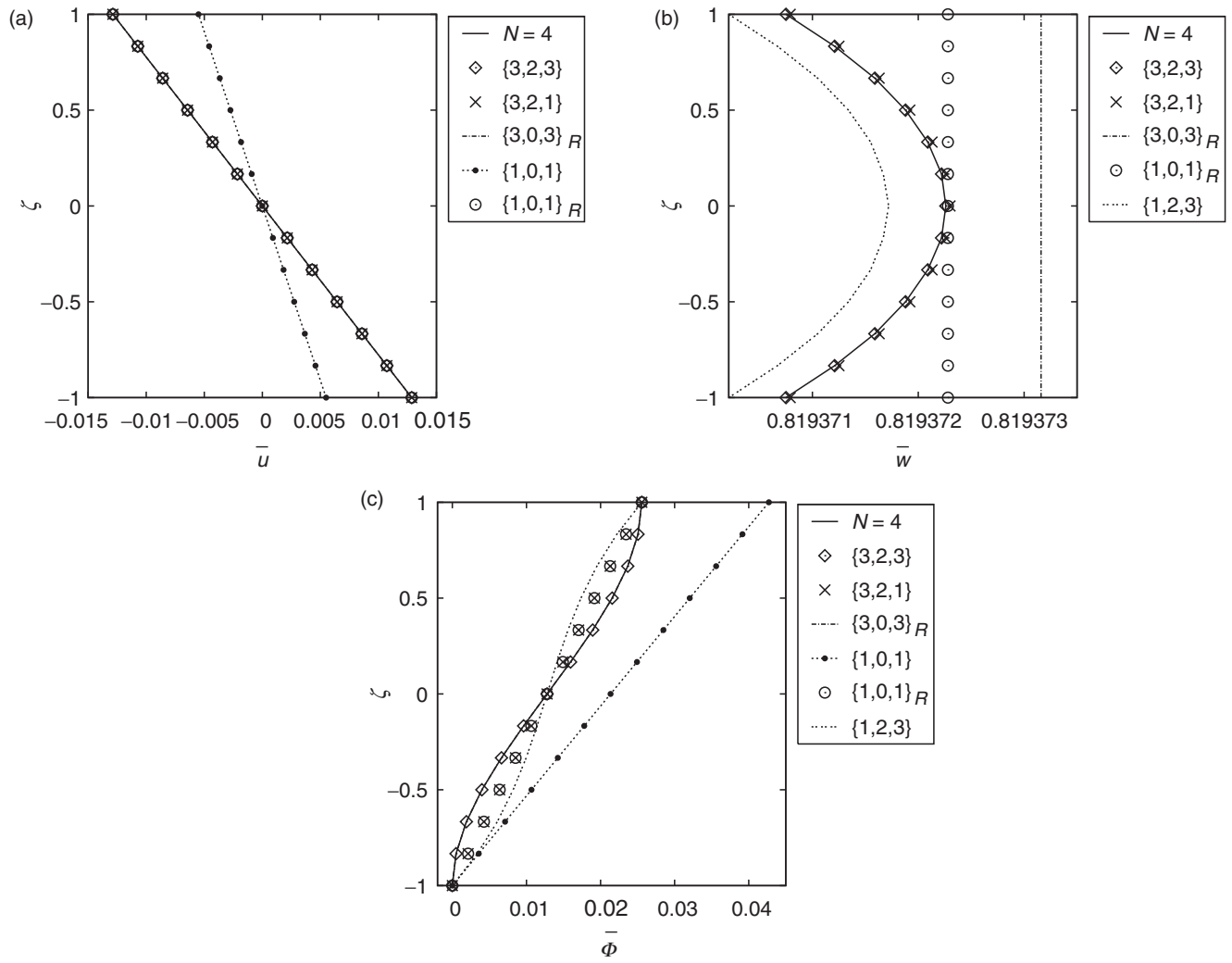

Figure 13. *Thin (S = 1000) sensor working in 15-mode: through-thickness distribution of the non-dimensional electromechanical response for selected* 2D *models: (a) In-plane displacement $\bar{u}$ (b) Transverse deflection $\bar{w}$ (c) Electrostatic potential $\bar{\Phi}$.*

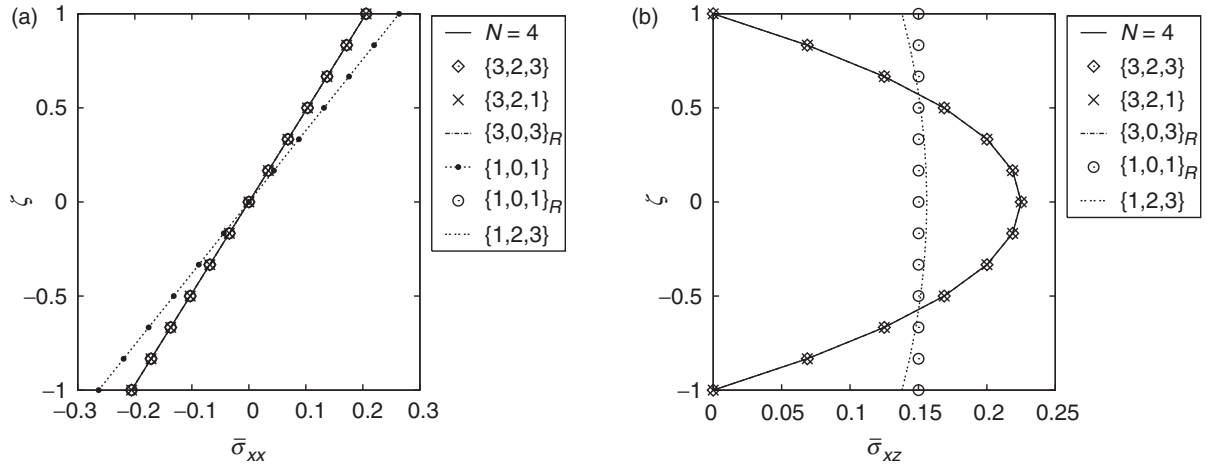

Figure 14. *Thin (S = 1000) sensor working in 15-mode: through-thickness distributions of the non-dimensional in-plane and transverse shear stresses for selected* 2D *models: (a) In-plane stress $\bar{\sigma}_{xx}$; (b) Transverse shear stress $\bar{\sigma}_{xz}$.*

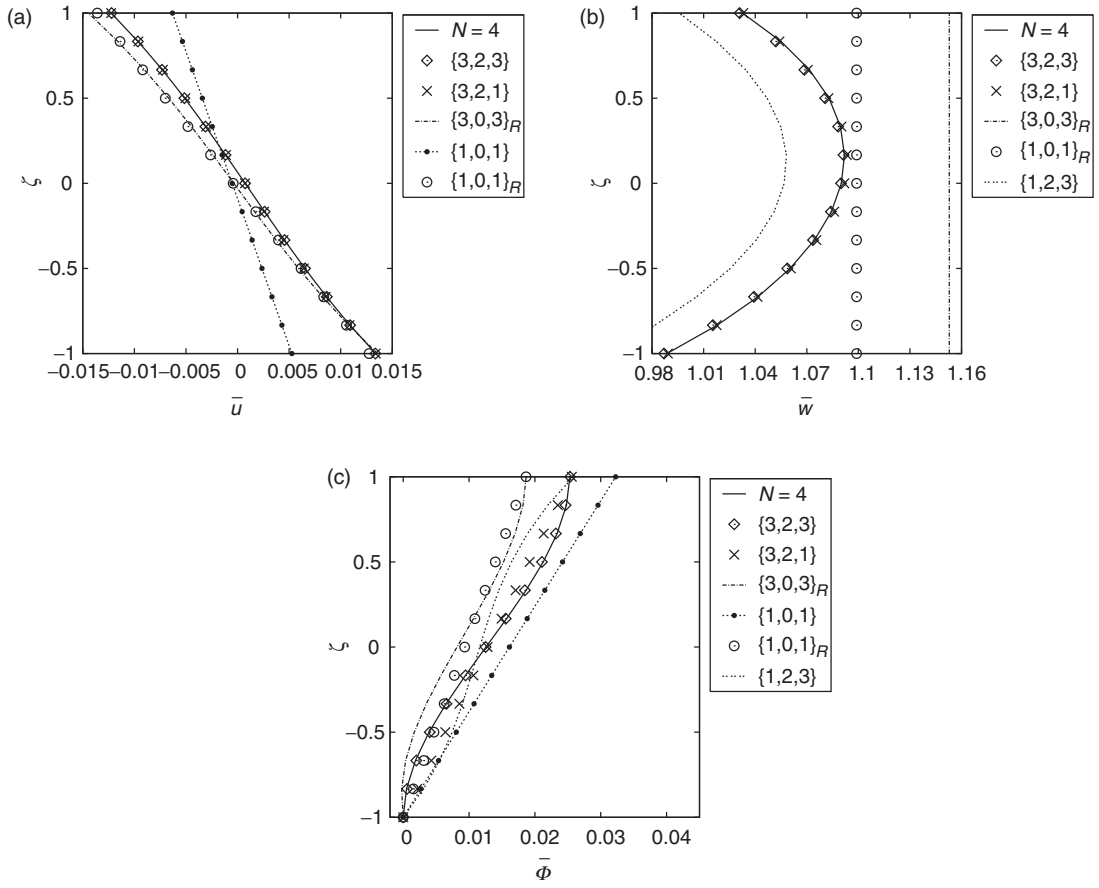

Figure 15. *Thick (S = 4) sensor working in 15-mode: through-thickness distribution of the non-dimensional electromechanical response for selected* 2D *models: (a) In-plane displacement $\bar{u}$; (b) Transverse deflection $\bar{w}$; (c) Electrostatic potential $\bar{\Phi}$.*

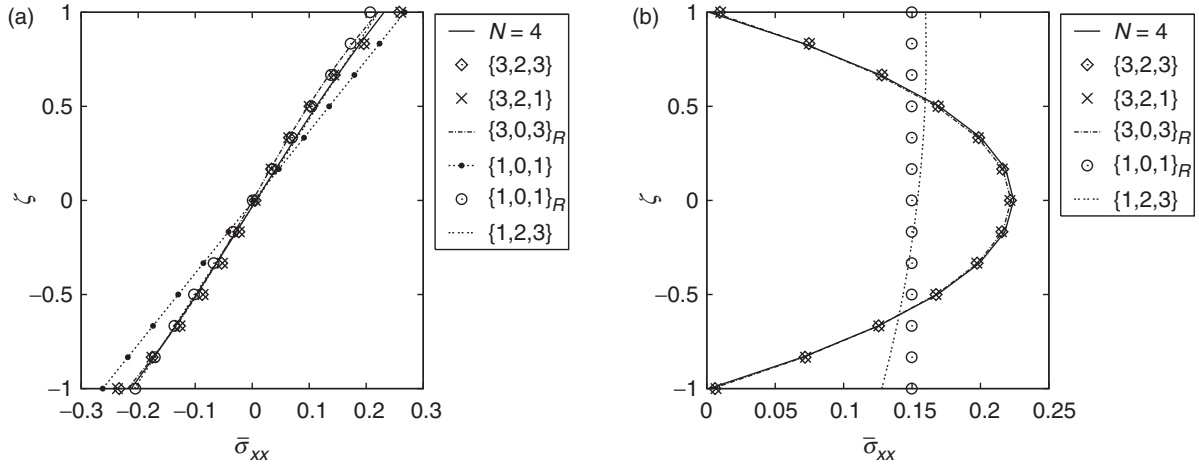

Figure 16. *Thick (S = 4) sensor working in 15-mode: through-thickness distributions of the non-dimensional in-plane and transverse shear stresses for selected* 2D *models: (a) In-plane stress $\bar{\sigma}_{xx}$; (b) Transverse shear stress $\bar{\sigma}_{xz}$.*

and asymmetric loading. The model $\{3, 2, 3\}$ captures considerably well the distributions of the displacements, electrostatic potential, and transverse shear stress. However, it slightly overestimates the maximum bending stresses σ_{xx}, see Figure 16(a). Since $N_u > N_w$, the in-plane strains ϵ_{xx}, ϵ_{yy}, and the transverse strain ϵ_{zz} define inconsistent contributions to the stress σ_{xx}. These inconsistencies become visible in thick 3D

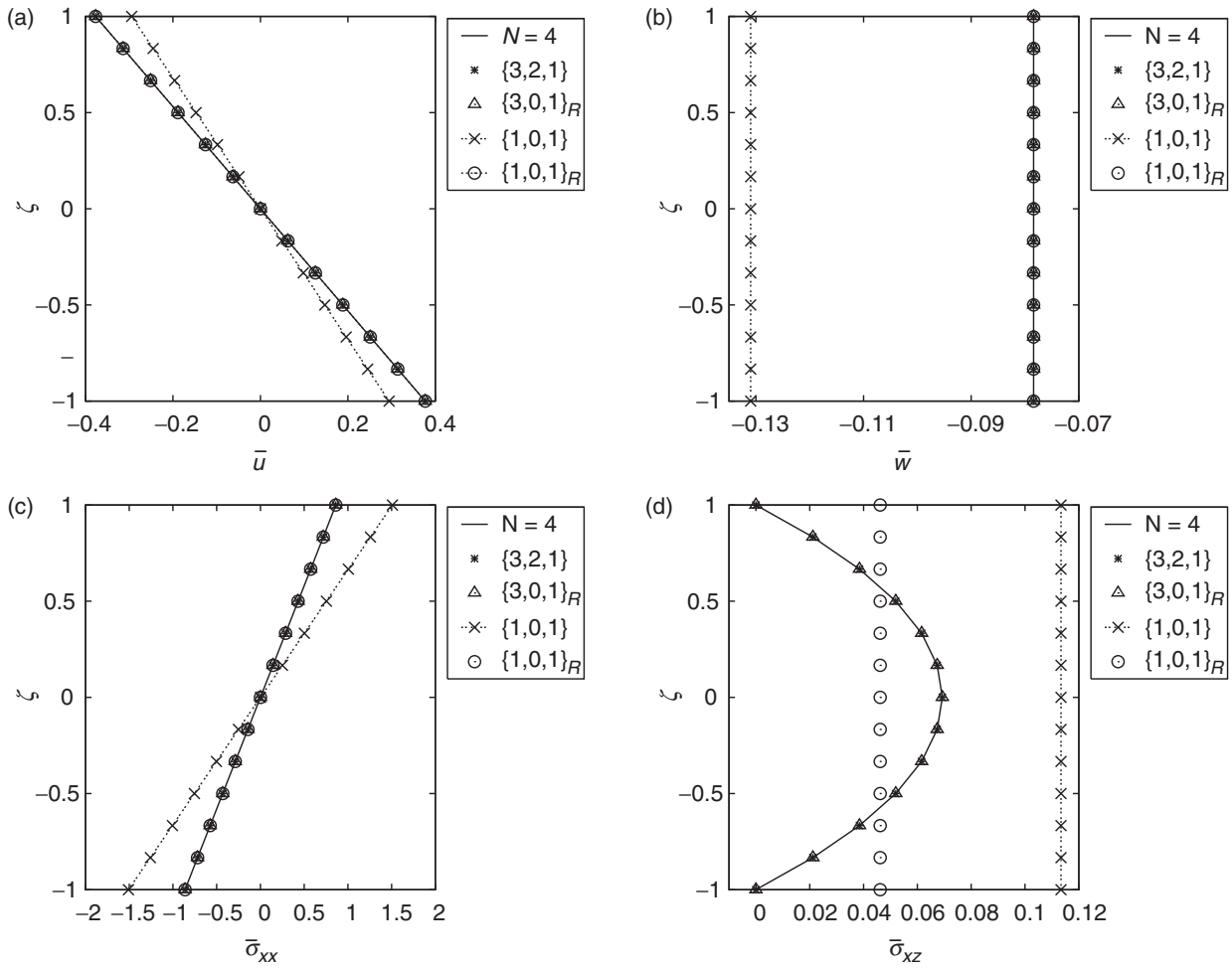

Figure 17. *Thin (S = 1000) piezoelectric shear actuator: through-thickness distributions of the mechanical in-plane and transverse response for selected* 2D *models: (a) In-plane displacement* $\bar{u}$*; (b) Transverse deflection* $\bar{w}$*; (c) In-plane stress* $\bar{\sigma}_{xx}$*; (d) Transverse shear stress* $\bar{\sigma}_{xz}$*.*

structures, for which the transverse direct strain ϵ_{zz} gains relevance with respect to the in-plane direct ('bending') strains ϵ_{xx} and ϵ_{yy}. The same behavior may have been noticed in Figure 7(c) for the thick sensor in 31-mode as well. This issue can be overcome by employing models with $N_w > N_u$ or by using $N_w = 0$ along with the reduced constitutive law. However, the use of reduced constitutive relations entails errors in the sensed voltage that are of the same order of magnitude of those produced by Poisson locking, see Figure 15(c).

By comparing Figures 13(c) and 15(c), it can be seen that the behavior of $\Phi(z)$ is identical for thin and thick plates. A non-linear (cubic) distribution along the thickness is obtained in either case, which confirms the validity of the hypotheses formulated by Trindade and Benjeddou (2006, 2008) for the construction of accurate models of shear-actuated piezoelectric sandwich beams. Indeed, the piezoelectric coupling *via* the e_{35} coefficient induces a quadratic distribution of $E_z = E_3$ as a consequence of the quadratic distribution of the transverse shear strain $\epsilon_{xz} = \epsilon_5$. Therefore, a quadratic approximation of the transverse shear strain (i.e., $N_u \geq 3$) is necessary to correctly resolve the piezoelectric interactions, even in presence of a classical bending response with a linear distribution of u. If the condition $N_w > N_u$ is retained, the model $\{3, 4, 3\}$ thus appears to be a consistent higher order model for thick sensors working in shear mode. As far as thin sensors are concerned, models with $N_w = 0$ and reduced constitutive equations can effectively capture the coupled piezoelectric response. Except for the direct computation of the transverse shear stress from the constitutive equations, the classical Reissner–Mindlin-based model $\{1, 0, 1\}_R$ is shown to provide satisfactory results.

Actuator Configuration

The piezoelectric response of a thin and thick piezoelectric actuator working in shear mode (see Figure 12(b)) is reported in Figures 17 and 18, respectively. The illustration of the through-thickness distribution of the electrostatic potential has been omitted for

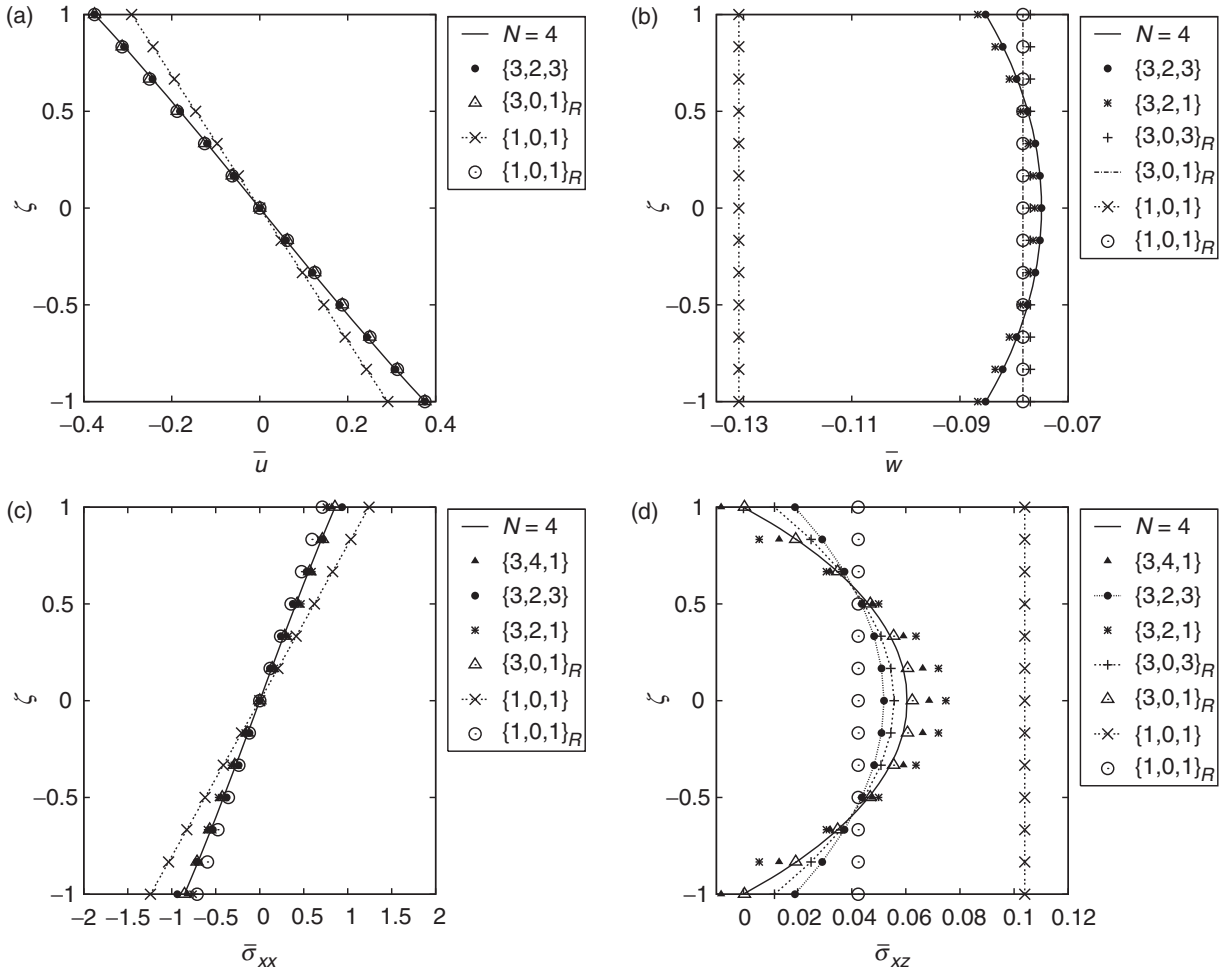

Figure 18. *Thick (S = 4) piezoelectric shear actuator: through-thickness distributions of the mechanical in-plane and transverse response for selected* 2D *models: (a) In-plane displacement $\bar{u}$; (b) Transverse deflection $\bar{w}$; (c) In-plane stress $\bar{\sigma}_{xx}$; (d) Transverse shear stress $\bar{\sigma}_{xz}$.*

brevity, identical considerations previously made for the actuator in 31-mode hold for the shear actuator. The results are reported in terms of the following non-dimensional parameters (Vel and Batra, 2001b):

$$\bar{u} = \frac{\tilde{C}_{55}}{e_{35}\Phi_0}\, u_x; \quad \bar{w} = \frac{\tilde{C}_{55}}{e_{35}\Phi_0\, S}\, w; \quad \bar{\sigma}_{xx} = \frac{hS}{e_{35}\Phi_0}\, \sigma_{xx};$$
$$\bar{\sigma}_{xz} = \frac{hS^2}{e_{35}\Phi_0}\, \sigma_{xz}; \quad \bar{\Phi} = \frac{1}{\Phi_0}\, \Phi. \tag{22}$$

Thanks to the employed non-dimensional factors, the electromechanical response of the shear actuator is invariant with respect to the aspect ratio $S = a/h$ of the plate.

The mechanical response to the symmetrically applied actuating field can be well described by a linear approximation for the in-plane displacement u. As already seen, the resulting linear distribution of in-plane direct strains requires an at least quadratic assumption for the transverse deflection in order to prevent Poisson locking. Note that the spurious stiffening due to Poisson locking (see the behavior of the model $\{1, 0, 1\}$) reduces the in-plane displacement and *increases the active deflection* w as well as the stress components. Introduction of the hypothesis $\sigma_{zz} = 0$ and use of the reduced constitutive law is shown to prevent Poisson locking without substantially affecting the accuracy of the response even in a thick actuator. The model $\{3, 0, 1\}_R$ proves particularly suitable for a refined representation of the transverse shear deformation.

CONCLUSIONS AND OUTLOOK

This article discussed a number of axiomatic plate theories for homogeneous piezoelectric actuators and sensors working either in extension mode (transverse polarization) or in shear mode (in-plane polarization). Various models have been assessed thanks to a unique software based on a GUF that permits to construct plate models with different polynomial approximations for the independent field variables. With reference to

Hamilton's principle for piezoelectric media, models have been formulated with different polynomial orders N_u for the in-plane displacement, N_w for the transverse displacement and N_Φ for the electrostatic potential. According to the presented results, the following piezoelectric models $\{N_u, N_w, N_\Phi\}$ can be recommended depending on the considered configuration:

- Actuator in 31-mode (extension actuation): accurate results can be obtained by the models $\{0, 1, 1\}$ and $\{2, 3, 3\}$ for thin and thick plates, respectively.
- Actuator in 15-mode (shear actuation): the global response can be well modeled with the assumptions $\{3, 2, 1\}$, but more refined models (e.g., $\{3, 2, 3\}$) are necessary for capturing the local transverse stress distribution.
- Sensor in 31-mode: the models $\{1, 2, 2\}$ and $\{3, 2, 2\}$ capture well the bending response and the induced electrostatic potential in thin and thick plates, respectively. The need for having $N_\Phi \geq 2$ has been confirmed.
- Sensor in 15-mode: the model $\{3, 2, 1\}$ yields satisfactorily results irrespective of the aspect ratio of the plate.

While all above models employ the full 3D constitutive law, lower-order models can be used that are based on the hypothesis $\sigma_{zz} = 0$ and the assumption $N_w = 0$. Present results indicate, however, that these models should not be used for thick sensor applications. The above recommendations are complemented with the following considerations:

- An accurate determination of transverse shear stresses directly from the constitutive law requires $N_u \geq 3$; lower-order models may be employed in conjunction with a post-processing step which calculates transverse stresses from, e.g., the equilibrium equations.
- The calculation of in-plane direct stresses from the constitutive law indicates that models with $N_w > N_u$ should be employed in case of thick structures.
- In actuator applications (i.e., prescribed voltage), the kinematics assumptions N_u, N_w do not influence the distribution $\Phi(z)$ of the electrostatic potential. While a linear approximation for $\Phi(z)$ proves sufficient for the global response, higher-order terms of this approximation affect the distribution of the actuating stress component (e.g., the in-plane stress σ_{xx} for the extension mode and the transverse shear stress σ_{xz} for the shear mode).

The presented results can serve as a useful guide for a consistent choice of axiomatic assumptions for the static analysis of piezoelectric plates. Further studies should extend the present methodology to different boundary conditions (e.g., clamped and free edges), to the analysis of dynamic problems and to multilayered structures. For this, it appears convenient to extend the promising GUF modeling so to account for electromechanical interfaces and an accurate local response analysis. The theoretical framework for this application being already available (Ballhause et al., 2005; D'Ottavio et al., 2008; D'Ottavio and Kröplin, 2006), these issues will be addressed in a forthcoming work.

REFERENCES

Aldraihem, O.J. and Khdeir, A.A. 2003. "Exact deflection solutions of beams with shear piezoelectric actuators," *Int. J. Solids Struct.*, 40:1–12.

Baillargeon, B.P. and Vel, S.S. 2005. "Active vibration suppression of sandwich beams using piezoelectric shear actuators: Experiments and numerical simulations," *J. Intellig. Mat. Sys. Struct.*, 16:517–530.

Ballhause, D., D'Ottavio, M., Kröplin, B. and Carrera, E. 2005. "A unified formulation to assess multilayered theories for piezoelectric plates," *Comput. Struct.*, 83:1217–1235.

Batra, R.C. and Aimmanee, S. 2003. "Missing Frequencies in Previous Exact Solutions of Free Vibrations of Simply Supported Rectangular Plates," *J. Sound Vibr.*, 265:887–896.

Batra, R.C. and Vidoli, S. 2002. "Higher-order Piezoelectric Plate Theory Derived from a Three-dimensional Variational Principle," *AIAA J.*, 40:91–104.

Batra, R.C., Vidoli, S. and Vestroni, F. 2002. "Plane Wave Solutions and Modal Analysis in Higher Order and Normal Deformable Plate Theories," *J. Sound Vibr.*, 257:63–88.

Benjeddou, A. 2000. "Advances in Piezoelectric Finite Element Modeling of Adaptive Structural Elements: a Survey," *Comput. Struct.*, 76:347–363.

Benjeddou, A. and Deü, J.-F. 2001. "Piezoelectric Transverse Shear Actuation and Sensing of Plates. Part 1: A Three-dimensional Mixed State Space Formulation. Part 2: Application and Analysis," *J. Intellig. Mat. Sys. Struct.*, 12:435–449. 12:451–467.

Benjeddou, A., Trindade, M.A. and Ohayon, R. 1997. "A Unified Beam Finite Element Model for Extension and Shear Piezoelectric Actuation Mechanisms," *J. Intellig. Mat. Sys. Struct.*, 8:1012–1025.

Bhaskar, K. and Varadan, T.K. 2001. "The Contradicting Assumptions of Zero Transverse Normal Stress and Strain in the Thin Plate Theory: A Justification," *J. Appl. Mech.*, 68:660–662.

Bisegna, P. and Maceri, F. 1996a. "A Consistent Theory of Thin Piezoelectric Plates," *J. Intellig. Mat. Sys. Struct.*, 7:372–389.

Bisegna, P. and Maceri, F. 1996b. "An Exact Three-dimensional Solution for Simply Supported Rectangular Piezoelectric Plates," *J. Appl. Mech.*, 63:628–638.

Büchter, N., Ramm, E. and Roehl, D. 1994. "Three-dimensional Extension of Nonlinear Shell Formulation Based on the Enhanced Assumed Strain Concept," *Int. J. Numer. Meth. Eng.*, 37:2551–2568.

Carrera, E. 2000. "An Assessment of Mixed and Classical Theories on Global and Local Response of Multilayered Orthotropic Plates," *Compos. Struct.*, 50:183–198.

Carrera, E. 2003. "Theories and Finite Elements for Multilayered Plates and Shells: A Unified Compact Formulation with Numerical Assessment and Benchmarking," *Arch. Comput. Meth. Eng.*, 10:215–296.

Carrera, E. and Brischetto, S. 2007a. "Piezoelectric Shells Theories with 'A Priori' Continuous Transverse Electro-mechanical Variables," *J. Mech. Mater. Struct.*, 2:377–399.

Carrera, E. and Brischetto, S. 2007b. "Reissner Mixed Theorem Applied to Static Analysis of Piezoelectric Shells," *J. Intellig. Mat. Sys. Struct.*, 18:1083–1107.

Carrera, E. and Brischetto, S. 2008a. "Analysis of Thickness Locking in Classical, Refined and Mixed Multilayered Plate Theories," *Compos. Struct*., 82:549–562.

Carrera, E. and Brischetto, S. 2008b. "Analysis of Thickness Locking in Classical, Refined and Mixed Theories for Layered Shells," *Compos. Struct*., 85:83–90.

Carrera, E., Giunta, G. and Brischetto, S. 2007. "Hierarchical Closed form Solutions for Plates Bent by Localized Transverse Loadings," *J. Zhejiang Univ. Sci. A*, 8:1026–1037.

Chao, P.C.-P. and Shen, C.-Y. 2007. "Dynamic Modeling and Experimental Verification of a Piezoelectric Part Feeder in a Structure with Parallel Bimorph Beams," *Ultrasonics*, 46:205–218.

Cheng, Z.-Q., Lim, C.-W. and Kitipornchai, S. 2000. "Three-dimensional Asymptotic Approach to Inhomogeneous and Laminated Piezoelectric Plates," *Int. J. Solids Struct*., 37:3153–3175.

Cho, M. and Oh, J. 2003. "Higher Order Zig-zag Plate Theory under Thermo-electric-mechanical Loads Combined," *Compos. B*, 34:67–82.

Chopra, I. 1996. "State-of-the-art of Smart Structures and Integrated Systems," In: Aatre, V.K., Varadan, V.K. and Varadan, V.V. (eds), *Symposium on Smart Materials, Structures, and MEMS*, Bangalore, India, SPIE Proceedings, Vol. 3321, pp. 2–44.

Chopra, I. 2002. "Review of State of Art of Smart Structures and Integrated Systems," *AIAA J*., 40:2145–2187.

Demasi, L. 2006. "Three-dimensional Closed form Solutions and Exact Thin Plate Theories for Isotropic Plates," *Compos. Struct*., 74:449–457.

Demasi, L. 2008. "∞^3Hierarchy Plate Theories for Thick and Thin Composite Plates: The Generalized Unified Formulation," *Compos. Struct*., 84:256–270.

D'Ottavio, M., Ballhause, D., Kröplin, B. and Carrera, E. 2006. "Closed-form Solutions for the Free-vibration Problem of Multilayered Piezoelectric Shells," *Comput. Struct*., 84: 1506–1518.

D'Ottavio, M., Wallmersperger, T. and Kröplin, B. 2008. "Classical and Advanced Models for Laminated Plates with Piezoelectric Layers Actuated in Shear Mode," *Mech. Adv. Mater. Struct*., 15:167–181.

D'Ottavio, M. and Kröplin, B. 2006. "An Extension of Reissner Mixed Variational Theorem to Piezoelectric Laminates," *Mech. Adv. Mater. Struct*., 13:139–150.

Fernandes, A. and Pouget, J. 2001. "Accurate Modelling of Piezoelectric Plates: Single-layered Plate," *Arch. Appl. Mech*., 71:509–524.

Fernandes, A. and Pouget, J. 2002. "An Accurate Modelling of Piezoelectric Multi-layer Plates," *Eur. J. Mech. Solids*, 21:629–651.

Fernandes, A. and Pouget, J. 2003. "Analytical and Numerical Approaches to Piezoelectric Bimorphs," *Int. J. Solids Struct*., 40:4331–4352.

Gaudenzi, P., Barboni, R. and Mannini, A. 1995. "A Finite Element Evaluation of Single-layer and Multi-layer Theories for the Analysis of Laminated Plates," *Compos. Struct*., 30:427–440.

Gaudenzi, P., Mannini, A. and Carbonaro, R. 1998. "Multi-layer Higher-order Finite Elements for the Analysis of Free-edge Stresses in Composite Laminates," *Int. J. Numer. Meth. Eng*., 41:851–873.

Gopinathan, S.V., Varadan, V.V. and Varadan, V.K. 2000. "A Review and Critique of Theories for Piezoelectric Laminates," *Smart Mater. Struct*., 9:24–48.

Heyliger, P.R. 1997. "Exact Solutions for Simply-supported Laminated Piezoelectric Plates," *J. Appl. Mech*., 64:299–306.

Heyliger, P.R. and Brooks, S. 1996. "Exact Solutions for Laminated Piezoelectric Plates in Cylindrical Bending," *J. Appl. Mech*., 63:903–910.

Kant, T. and Shiyekar, S.M. 2008. "Cylindrical Bending of Piezoelectric Laminates with a Higher Order Shear and Normal Deformation Theory," *Comput. Struct*., 86:1594–1603.

Mannini, A. and Gaudenzi, P. 2004. "Multi-layer Higher-order Finite Elements for the Analysis of Free-edge Stresses in Piezoelectric Actuated Laminates," *Compos. Struct*., 63:263–270.

Maugin, G.A. and Attou, D. 1990. "An Asymptotic Theory of Thin Piezoelectric Plates," *Quart. J. Mech. Appl. Math*., 43:347–362.

Naghdi, P.M. 1972. "The Theory of Shells and Plates," In: Flügge, S. and Truesdell, C. (eds), *Handbuch der Physik*, Vol 6a, pp. 425–640, Springer-Verlag, Berlin.

Paumier, J.-C. and Raoult, A. 1997. "Asymptotic Consistency of the Polynomial Approximation in the Linearized Plate Theory. Application to the Reissner-Mindlin Model," In: *ESAIM: Proceedings*, Vol. 2, EDP Sciences, pp. 203–213.

Pietrzakowski, M. 2008. "Piezoelectric Control of Composite Plate Vibration: Effect of Electric Potential Distribution," *Comput. Struct*., 86:948–954.

Polit, O. and Bruant, I. 2006. "Electric Potential Approximations for an Eight Node Plate Finite Element," *Comput. Struct*., 84:1480–1493.

Raja, S., Sreedeep, R. and Prathap, G. 2004. "Bending Behavior of Hybrid-actuated Piezoelectric Sandwich Beams," *J. Intellig. Mat. Sys. Struct*., 15:611–619.

Reddy, J.N. 1999. "On Laminated Composite Plates with Integrated Sensors and Actuators," *Eng. Struct*., 21:568–593.

Reddy, J.N. 2004. *Mechanics of Laminated Composite Plates and Shells: Theory and Analysis*, 2 edn, CRC Press, Boca Raton, FL.

Reddy, J.N. and Cheng, Z.-Q. 2001. "Deformations of Piezothermoelastic Laminates with Internal Electrodes," *ZAMM*, 81:347–359.

Robbins Jr, D.H. and Chopra, I. 2006. "The Effect of Laminate Kinematic Assumptions on the Global Response of Actuated Plates," *J. Intellig. Mat. Sys. Struct*., 17:273–299.

Roccella, S. and Gaudenzi, P. 2005. "On the Formulation of a Piezoelectric Plate Model," *J. Intellig. Mat. Sys. Struct*., 16:285–290.

Rogacheva, N.N. 1994. *The Theory of Piezoelectric Shells and Plates*, CRC Press, Boca Raton.

Saravanos, D.A. and Heyliger, P.R. 1999. "Mechanics and Computational Models for Laminated Piezoelectric Beams, Plates and Shells," *Appl. Mech. Rev*., 52:305–319.

Sun, C.-T. and Zhang, X.D. 1995. "Use of Thickness-shear Mode in Adaptive Sandwich Structures," *Smart Mater. Struct*., 4:202–206.

Sze, K.Y., Yang, X.-M. and Fan, H. 2004. "Electric Assumptions for Piezoelectric Laminate Analysis," *Int. J. Solids Struct*., 41:2363–2382.

Tiersten, H.F. 1969. *Linear Piezoelectric Plate Vibrations*, Plenum, New York.

Trindade, M.A. and Benjeddou, A. 2006. "On Higher-order Modelling of Smart Beams with Embedded Shear-mode Piezoceramic Actuators and Sensors," *Mech. Adv. Mater. Struct*., 13:357–369.

Trindade, M.A. and Benjeddou, A. 2008. "Refined Sandwich Model for the Vibration of Beams with Embedded Shear Piezoelectric Actuators and Sensors," *Comput. Struct*., 86:859–869.

Trindade, M.A., Benjeddou, A. and Ohayon, R. 1999. "Parametric Analysis of the Vibration Control of Sandwich Beams through Shear-based Piezoelectric Actuation," *J. Intellig. Mat. Sys. Struct*., 10:377–385.

Vel, S.S. and Batra, R.C. 2001a. "Analysis of Piezoelectric Bimorphs and Plates with Segmented Actuators," *Thin-Wall. Struct*., 39:23–44.

Vel, S.S. and Batra, R.C. 2001b. "Exact Solution for the Cylindrical Bending of Laminated Plates with Embedded Piezoelectric Shear Actuators," *Smart Mater. Struct*., 10:240–251.

Wang, J. and Yang, J.S. 2000. "Higher-order Theories of Piezoelectric Plates and Applications," *Appl. Mech. Rev*., 53:87–99.

Zhang, X.D. and Sun, C.-T. 1996. "Formulation of an Adaptive Sandwich Beam," *Smart Mater. Struct*., 5:814–823.

Zhang, X.D. and Sun, C.-T. 1999. "Analysis of a Sandwich Plate Containing a Piezoelectric Core," *Smart Mater. Struct*., 8:31–40.